Cheminformatic identification of small molecules targeting acute myeloid leukemia

Megan R. Daneman*[1], Bernadetta Meika*[1], Elissa Tjahjono[1], Alexey V. Revtovich[1], Leonid A. Stolbov[2], Scott R. Gilbertson[3], Vladimir V. Poroikov[2], Natalia V. Kirienko[#1]

[1]Department of BioSciences, Rice University, Houston, TX, USA.

[2]Institute of Biomedical Chemistry, Moscow, Russia.

[3]Department of Chemistry, University of Houston, 3585 Cullen Blvd. #112, Houston, TX 77004, USA.

*Contributed equally.

[#]Corresponding author. Department of BioSciences, Rice University, Houston, TX, USA. kirienko@rice.edu.

Abstract

Acute myeloid leukemia (AML) is an aggressive hematological malignancy that has poor prognosis and high relapse rates with cytotoxic chemotherapeutics. Previously, we identified modulators of mitochondrial function, PS127-family compounds, that were cytotoxic to AML and were characterized by two predicted functions: apoptotic agonism and thioredoxin/glutathione reductase inhibition (T/GRi). Here, we uncovered a third critical predicted function: autophagic induction. A cheminformatics screening of ~4.2 million compounds for molecules with high probability of these three functions yielded 93 hits, 81 of which were closely related to PS127-family molecules. *In silico* hits selected for validation selectively killed AML cells, activated apoptosis, required functional autophagy, and interfered with glutathione metabolism, confirming predicted functions. This increased pools of cytosolic and mitochondrial ROS and decreased oxygen consumption and ATP synthesis. Differential scanning fluorimetry implicated glutathione

reductase as a direct target of these molecules. Structurally-unrelated compounds from different clusters caused the same phenotype, validating our structure-blind screening approach. Furthermore, strong synergy between these compounds and the AML treatment midostaurin underscores their therapeutic potential.

Introduction

Acute myeloid leukemia (AML) is an aggressive, heterogeneous hematopoietic malignancy that is fatal when left untreated. AML occurs when hematopoietic stem cells mutate, causing immature myeloid precursor cells to divide uncontrollably. Rapid division of myeloid precursors decreases the number of healthy immune cells and differentiation, leading to immunosuppression and making the patients susceptible to diseases, including opportunistic pathogens (1). Additionally, the 5-year survival rate decreases with increasing patient age and the number of comorbidities, as these patients are less tolerant of intensive treatments (2). Therefore, fast diagnosis and effective treatment are crucial for patient survival.

In addition to low tolerance of current chemotherapy regimens, cancerous AML cells develop resistance mechanisms. The heterogeneous population of AML cells provides an opportunity for relapse after remission due to primary (before drug administration) or acquired drug resistance (after drug administration). Multidrug resistance (MDR) genes are involved in efflux, influx, proliferation, and anti-apoptotic pathways (3). For example, multidrug resistance-related protein (MRP1/ABCC1), promotes drug resistance by transporting drugs outside the cell and isolating drugs in vesicles (3,4). However, MRP1 can also cause efflux of the antioxidant glutathione (GSH), increasing cellular sensitivity to reactive oxygen species (ROS) levels (4,5).

The intricate balance of detoxification and resource production that modulate ROS levels provides a therapeutic opportunity to tip the scales by targeting mitochondrial metabolism.

The mutation profiles of AML are also important to consider when administering and developing new chemotherapeutics. Proto-oncogenes, which are necessary for cell proliferation, can mutate into oncogenes to induce tumorigenesis (6). However, they can also be a target for drug design. The most common mutation, which occurs in about 30% of AML patients, is the cell proliferation marker, Fms-like tyrosine kinase 3 (FLT3). This mutation typically occurs as an internal tandem duplication (ITD) or tyrosine kinase domain (TKD) mutation (7–9). FLT-ITD is associated with poor prognosis due to increased or constitutively activated cell proliferation. Current FLT3-ITD inhibitors, such as midostaurin, quizartinib, gilteritinib, and sorafenib, are subject to resistance due to FLT3 point mutations (3,10–16). Therefore, when investigating potential novel therapeutic targets, metabolic pathways and bioenergetics are a promising start.

AML is driven from two populations: immature myeloblasts and leukemic stem cells (LSCs) (17,18). Myeloblasts are targeted with front-line induction and consolidation treatments comprised of a pyrimidine analog arabinose-C/cytarabine (ara-C) and an anthracycline drug, but this regimen is insufficient for LSCs elimination. LSCs divide slowly, while myeloblasts divide rapidly. Therefore, LSCs are less sensitive to the anti-proliferative mechanisms of first-line chemotherapeutics. However, notably these two leukemic cell populations undergo metabolic reprogramming that makes their mitochondria sensitive to damage, revealing a way to target both populations (19).

AML cells favor oxidative phosphorylation (OXPHOS) and glutaminolysis (17,18,20–22). Increased OXPHOS enhances production of ROS, making cells more sensitive to mitochondrial damage. The heterogenous nature of AML cell populations also contain cells that are less effective

at ATP production due to low coupling efficiency (23,24). Substantial mitochondrial damage often leads to mitophagy, or the recycling of dysfunctional or damaged mitochondria. This process must be heavily regulated to maintain homeostasis. It has been shown that both the induction and inhibition of mitophagy induce leukemia cell death (7,17,25–27). Similarly, upregulation of mitophagy can induce resistance to chemotherapeutics such as venetoclax; however, upregulation of mitophagy pathways have been shown to correlate to increased patient survival, making mitophagy a great potential therapeutic target for AML treatment (28,29).

Our study took advantage of the metabolic reprogramming AML cells undergo by targeting their partially dysfunctional mitochondria with compounds that disrupt mitochondrial homeostasis (23). Previously, we discovered that mitochondria in AML cells have lower coupling efficiency, likely due to a higher proton leak (30). Consequently, it made AML cells highly sensitive to multiple combination of mitochondria-targeting drug with an established AML treatment (31). A panel of novel activators of PINK1-mediated mitophagy was previously discovered using a phenotypic screen in the nematode *Caenorhabditis elegans* (32). These PINK1-Stabilizing (PS) compounds increased levels of PINK1 in *C. elegans* and notably, selectively killed AML cells (23). These compounds also interfered with mitochondrial bioenergetics, characterized by decreased routine and ATP-linked respiration, and increased mitochondrial membrane depolarization—ultimately leading to cell death in blasts and LSCs. Cheminformatic analysis revealed that the most promising compounds, PS127E and PS127B, were likely inhibitors to key enzymes responsible for redox homeostasis (23).

In this manuscript, we used ligand-based cheminformatics approach to screen over 4.2 million compounds to identify small molecules with the same probable functions as mitophagic activators from the PS127 family. Specifically, the presence of these three functions: apoptosis

agonism, thioredoxin or glutathione reductase inhibition (T/GRi), and autophagic induction, was sufficient to selectively kill AML cells. Ninety-three such hits were discovered, with 81 clustering with our prior hits from PS127 family. These compounds were found to be synergistic with chemotherapeutics, particularly midostaurin (MID), indicating their potential as combinatorial treatment for AML. To uncover their mechanism of action, we verified these three predicted activities of selected PS127 analogs. We demonstrated that these compounds triggered apoptosis, required functional autophagy for AML cell cytotoxicity, and affected glutathione metabolism. Importantly, we identified glutathione reductase (GSR) as a molecular target of these compounds and demonstrated evidence of drug-target interaction. A structurally unrelated hit, compound 125_1, yielded very similar experimental outcomes, validating our approach. Compounds from the PS127 family and 125_1 negatively affected mitochondrial metabolism in AML cells, resulting in lower oxygen consumption rates (OCR) and concomitant decrease in ATP levels. These findings showed that using cheminformatics to screen for specific functions based on bioactive molecules is valuable in identifying novel compounds.

METHODS

Cell culture, AML cell lines, PBMCs, and treatments

AML cell lines (MOLM-13, MOLM-14, MV4-11, THP-2, and OCI-AML2) were purchased from ATCC (Manassas, VA, USA). MOLM-13 was used as our main AML cell line model, unless specified otherwise, to assess compound cytotoxicity and mechanisms of action. Cell cultures were maintained in RPMI-1640 medium supplemented with 2 mM L-glutamine and sodium bicarbonate (Sigma-Aldrich), 10% Corning^{TM} Regular Fetal Bovine Serum (FBS) (Heat Inactivated) and 1%

penicillin-streptomycin solution (P/S) (Sigma-Aldrich) in a 37°C humidified atmosphere with 5% CO_2.

Peripheral blood mononuclear cells (PBMCs) were obtained from the Gulf Coast Regional Blood Centre (Houston, TX, USA). PBMCs were used to represent healthy cells as a counterpart to AML cells and to assess for selectivity against AML cells over healthy cells. Healthy PBMCs were isolated using Ficoll®-Paque PREMIUM (Cytiva) according to manufacturer's instructions. PBMCs were maintained overnight (at least 16 hours) at a minimum density of 10^6 cells/mL before experimental use. All molecules that were identified *in silico* were purchased from Molport (www.molport.com). Each *in silico*-identified compounds, commercial chemotherapeutics, and antioxidants were prepared as a 10 mM stock solution in DMSO or sterile water, aliquoted, and stored at -20°C. Compounds were stored for short-term use at 4°C.

In silico screen

Chemoinformatics analysis was performed using Prediction of Activity Spectra for Substances (PASS) version 2022 (33). Database of ~4.2 million molecules was screened for identified activities with PASS using $\Delta P \geq 0.7$. ΔP represents the prediction of activity (Pa) minus the prediction of inactivity (Pi) (33). The remaining molecules (n = 161) were clustered based on structural similarity using Multidimensional Scaling (MDS) in ChemMine Tools (cut off ≥ 0.4) (34). A second filtration of the 161 molecules resulted in 93 molecules was done using autophagic induction PASS activity ($\Delta P \geq 0.7$). Structural similarity was analyzed further using the Tanimoto coefficient based on PubChem fingerprinting and visualized in Cytoscape 3.10.3.

Cytotoxicity assay

Cell viability was assessed by seeding cells at a density of 5,000 AML cells or 50,000 PBMCs per well into 96-well plates. Preliminary cytotoxicity assays assessed compound efficacy at 10 µM of compound. Cells were treated with compounds or solvent controls for 72 hours with a final volume of 100 µL in experimental media (RPMI-1640 with 1% FBS, 1% P/S). After 72 hours of treatment, cells were stained with Hoechst 33342 and propidium iodide (PI) to detect total and dead cells, respectively, as previously described (35). Plates were spun down for 5 minutes at 1,000 rcf in the Hermile Z446 Benchmark. Stained cells were then analyzed on a BioTek plate reader (Cytation 5 Cell Imaging Multi-Mode Reader) with Gen5 software.

The concentration of 50% cytotoxicity (CC_{50}) for each compound was determined by fitting dose-response models using the dose-response curve (drc) package in R (36). Cells were seeded in 96-well plates and immediately treated with compound or the solvent control, DMSO, at 5,000 AML cells/well or 50,000 PBMCs/well. Cell viability assays were performed using a 2-fold serial dilutions in a 96-well plate. The highest concentration of solvent control was used, never exceeding 0.5% (v/v). Cell viability was normalized to the solvent-control viability. Three technical replicates were performed per dose with at least three biological replicates.

Compound synergy assay

Combination cell viability was assessed by following previously described guidelines (31). We assessed the synergistic potential of three commercially used AML chemotherapeutics: doxorubicin (DOX) (Ark Pharm Inc.), cytarabine (ara-C) (Accela Chembio Inc), and midostaurin (MID) (MedChemExpress) to capture how our PS127-family compounds would interact with first-line chemotherapeutics and targeted therapy.

Cells were seeded at a density of 5,000 AML cells or 50,000 PBMCs per well into 96-well plates and immediately treated with a commercial chemotherapeutic and PS127-family compound with a final volume of 100 µL in experimental RPMI-1640 media (1% FBS, 1% P/S). Cells were treated for 72 hours using a concentration matrix starting at approximately 2-fold of the 72-hour CC_{50} values, followed by three 2-fold serial dilutions. The single treatment concentrations were also included in the matrix. Single drug treatments and combinations were assessed in technical duplicates per each of three biological replicates. Due to differences in final DMSO volume from various final drug1/drug2 combination, the highest DMSO amount was used as a solvent-control. All viability was normalized to the DMSO control viability. Plates were imaged for viability using the BioTek plate reader with Hoechst/PI double-staining.

Synergy for each biological replicate was determined by inputting the cell viability and corresponding drug1/drug2 concentrations into the SynergyFinder package in R (https://synergyfinder.fimm.fi) (37). Synergy scores were calculated using Bliss model. According to this model, Bliss synergy scores indicate that scores larger than 10 are synergistic, while scores between -10 and 10 are additive, and scores below -10 are antagonistic. We further categorized synergistic strength as follows: low synergy (10-20), medium synergy (>20-30), and high synergy (>30). Synergy plots were created using the same package and visualized in a 2D format. We determined the synergistic potential of our compounds by taking the average max synergy scores from at least three biological replicates. Corresponding PBMC synergy matrices were performed to assess potential synergy in healthy cells. Synergy graphs shown are representative of one biological replicate.

Evaluation of T/GRi activity

To assess thioredoxin reductase (TrxR) activity, MOLM-13 cells seeded at density of 10^6 cells/mL were treated with PS127-compound at $CC_{50,\ 72hours}$ for 48 hours. DMSO was used as negative control. Cell lysates were then prepared and assessed using the Thioredoxin Reductase Colorimetric Assay Kit (Cayman Chemicals) at 414 nm according to manufacturer's instructions. PS127-treated sample, positive control, and solvent-control were assessed in duplicate.

The ratio of reduced glutathione (GSH) to oxidized glutathione (GSSG) was assessed using the EnzyChrom™ Glutathione GSH/GSSG Assay Kit. MOLM-13 cells were treated with similar conditions as above. Samples were prepared following manufacturer's instructions for GSSG and total glutathione measurements. The amount of GSSG and total glutathione was determined from OD_{412nm} measurements at 0 and 10 minutes. Concentration of GSH or GSSG was normalized to total protein concentration, determined by Pierce™ BCA Protein Assay Kit, and negative control.

Assessment of autophagy-inducing activity

The ability for PS127-compounds to induce cytotoxicity through inducing autophagy was assessed by co-treating MOLM-13 cells with known autophagy inhibitor, 3-methyladenine (3-MA) (TCI America™) (38). Cell viability was assessed as a matrix of PS127-compound and 3-MA single and combined treatment. MOLM-13 cells were seeded at a density of 5,000 cells per well at the concentration matrixes described **in Figure 4C and S8A** for 24 hours. Plates were stained with Hoechst/PI and visualized in the BioTek plate reader.

Supplementation of exogenous antioxidants

The concentration in which antioxidant would not induce cell death was determined for each antioxidant used to supplement compound treated cells **(Figure S9).** We found that exogenously

supplementing GSH (Thermo Scientific Chemicals) and GSSG (TCI America™) was not toxic to MOLM-13. However, tocopherol (Thermo Scientific Chemicals) and ascorbate (TCI Chemicals) were toxic at concentrations higher than 62.5 µM and 15.63 µM respectively. These concentrations were then used in subsequent combination assays. GSH, GSSG, tocopherol and ascorbate were dissolved in sterile water.

MOLM-13 cells were simultaneously treated with antioxidants and tested compounds at their 4X CC_{50} for 72 hours to assess rescue of cell viability. Cell viability was assessed with Hoechst/PI staining in the BioTek plate reader as described previously.

Flow Cytometry

Total and mitochondrial ROS were measured using dihydroethidium (DHE) (Invitrogen™) or MitoSOX™ Red (Invitrogen™) staining, respectively, as described in manufacturer's protocols. Cells were double stained with Hoechst as viability control. Meanwhile, Annexin V-FITC/PI/Hoechst staining was used to detect live, apoptotic, and dead cells as previously described (23). For each experiment, MOLM1-13 were seeded at a density of 10^6 cells/mL and treated with 8 µM of screened compound or 4 µM of PS127_10 for 24 hours. DMSO was used as negative control. Flow cytometry was performed on SONY MA900 Cell Sorter. Data were analyzed in FlowJo software 10.8.1.

Differential Scanning Fluorometry (DSF)

DSF was performed by combining final concentrations of 5 µM of human glutathione reductase (GSR) (Sigma-Aldrich), 20 µM of each compound, and 5X of SYPRO® Orange Protein Gel Stain (ThermoFisher). The total final volume per well was 20 µL. Buffer solution used to dilute

compound and GSR stocks was 20 mM HEPES, pH 7.4, 100 mM NaCl with 1% DMSO (39). We included no protein controls, compound-fluoresce interference controls, and autofluorescence plate controls. The known GSR inhibitor, 2-AAPA (Sigma-Aldrich), was used as a positive experimental control. After being sealed with clear adhesion covers, PCR plates were continuously heated with gradual increase in temperature from 25°C to 95°C at 1-minute intervals using the PREP BioRad qPCR instrument. RFU was then determined through the FRET channel. Melting temperature was determined by the derivative of relative fluorescence units (dRFU) using the open access tool, DSFworld (40).

Oxygen consumption rate measurements

Oxygen consumption rate (OCR) and oxygen concentration were measured using the NextGen-O2k instrument (Oroboros Instrument, Innsbruck, Austria). Additional modules required for various experiments were assembled and used (e.g. SmartPOS, TIP-2k). Instrumental background calibration with MiR05 (Oroboros) and oxygen air calibration with experimental media (RPMI-1640 supplemented with 1% FBS and 1% P/S) were performed according to standardized protocols. The oxygen solubility factor was altered based on media used in chamber (0.92 for MiR05, 0.89 for RPMI) at 37ºC. Measurements were taken every 2 seconds.

OCR was determined using oxygen detecting protocols provided by Oroboros. Routine respiration was assessed in live cells (≥ 90% viability) using 2-mL Duran® glass chambers filled with experimental RPMI-1640 medium, maintained at 37°C, and stirred at 750 rpm. Live cells were incubated for 3 hours with 4 µM compound treatment or corresponding volume solvent control (DMSO) at 10^6 cells/mL in a 6-well plate in a humidified 37°C incubator with 5% CO_2. Cell concentration and viability were measured with the Invitrogen Countess II Automated Cell

Counter using Trypan-Blue (0.4%) before treatment and after oxygen measurement. The OCR was calculated from the average of oxygen negative slope over time normalized to total number of cells per chamber volume using the data analysis template Excel file provided by Oroboros.

ATP measurements

MOLM-13 cells were seeded at a density of 5,000 cells per well into an opaque 96-well plate and incubated with either 4 µM compound or corresponding volume of solvent control (DMSO) for 3 hours at a final volume of 100 µL of experimental RPMI medium. Each biological replicate was analyzed in three technical replicates. Cells were double-stained with Hoechst/PI to assess cell viability as previously described. Each well was maintained to have greater than 90% viability before proceeding with cell lysis. After imaging, plate was spun down again for 5 minutes and 50 µL of media was removed from each well. Subsequently, 50 µL of CellTiter-Glo® 2.0 (Promega) solution was added to each well. Plate was then kept in the dark, gently shaken for 1 minute to induce cell lysis, and incubated at room temperature for 10 minutes to allow luciferase activation. The luciferase signal was measured via luminescence on the BioTek plate reader (Cytation 5 Cell Imaging Multi-Mode Reader) with Gen5 software. The total ATP production was then calculated by dividing the luminescence signal by the total number of live cells per well.

RESULTS

In silico biological activity screen identifies AML-targeting compounds

Previous research in our lab identified PS127 as a novel activator of mitophagy (32). Subsequent study demonstrated that this molecule selectively kills AML cells. A small-scale structural similarity search and structure-activity relationship analysis identified ~15 analogs of

PS127, 12 of which showed cytotoxicity against AML *in vitro* (23). In order to identify potential mechanisms of action for these molecules, a chemoinformatics software package called Prediction of Activity Spectra for Substances (PASS) was used (41). PASS uses a set of interest with chemical structures of drug-like compounds to predict a range of biological activities. Probability to be active (Pa) and to be inactive (Pi) are shown for specific molecule. Both of them are ranged between 0 (no likelihood of activity) and 1 (high likelihood of activity). Pa scores above 0.7 indicate a high probability of compound activity (33). PASS analysis predicted that all 12 active PS127-analogs had high probability for two activities: apoptotic agonism and thioredoxin / glutathione inhibition functions (T/GRi) (23). These activities were specific to active molecules; analogs found to lack activity *in vitro* (such as PS127H) had low Pa scores for these activities (**Figure 1A**).

These results suggested that the ability of PS127-family molecules to selectively kill AML cells was linked to at least one of these predicted functions. To identify additional molecules with these predicted functions, an *in silico* screen of over 4.2 million compounds was performed. To increase stringency and reduce the number of false positive hits, the screen parameters were adjusted. Compounds were considered hits only if ΔP (defined as Pa – Pi) was at least 0.7 for each of the desired activities (**Figure 1B**). This screen yielded a set of 161 potential hits (**Figure 1B**). The molecules were grouped into 41 clusters based on structural similarity using multidimensional scaling (MDS) (**Figure 1C and Figure S1**). This process identified two large clusters with structurally-related compounds, referred to here as clusters 20 and 103.

Cluster 20 contained 82 compounds, including multiple previously-identified PS127-family hits, like PS127E and PS127B. This group will henceforth be referred to as the PS127-family cluster. A subset of 14 compounds from this cluster were ordered and tested as representatives of

297 the PS127-family cluster's chemical space (**Figure 1D**). Compounds were dissolved in DMSO
298 and tested for cytotoxicity in an AML cell line, MOLM-13, at 10 μM for 72 hours (**Figure 1E**).
299 All PS127-family compounds tested showed high cytotoxicity to the AML cells (**Table 1**).

300 Cluster 103 was comprised of 18 molecules, four of which were ordered and tested as above
301 (**Figure 1E**). None showed activity *in vitro*, despite being predicted to have the same two activities.
302 Tanimoto-based structural analysis showed that all cluster 103 compounds had high structural
303 similarity to each other (Tanimoto coefficient ≥ 0.75), whereas compounds from PS127-family
304 cluster formed distinct sub-clusters (**Figure S2, Table S1**). For example, PS127_10 and PS127E
305 were more structurally similar to each other (Tanimoto coefficient 0.833) than they were to
306 PS127_4 or PS127_6, which were more closely related to each other (Tanimoto coefficient
307 0.0758).

308 To gain insight into the basis for functional differences between compounds from these two
309 clusters, active and inactive compounds were reassessed with the PASS software. This revealed
310 several additional activities unique to active, PS127-family molecules. The most intriguing of
311 these was autophagic induction, a feature we have previously linked to mitochondrial health and
312 AML sensitivity to drugs (23,30). We hypothesized that this third activity was required for
313 cytotoxicity and may be differentiating active and inactive compounds in our 161 hits. When
314 applied to this set, the number of hits was narrowed to 93 molecules, excluding all of the
315 compounds in cluster 103 (**Figure 1F**). Of these 93 molecules, 81 molecules belonged to the
316 PS127-family cluster, while the remaining 12 were structurally distinct from this group. Five of
317 these 12 compounds were selected and tested for cytotoxicity in MOLM-13 cells (**Figure 1G**).
318 Four molecules significantly reduced AML cell viability. Overall, 125_1, 16_2, and 141_1 were
319 structurally unrelated to each other or PS127-family, but cytotoxic to AML cells. These data

corroborated our hypothesis that the presence of these three predicted functions underlying AML cytotoxicity, providing proof of principle.

PS127 family has selective cytotoxicity against AML cell lines

After initial cytotoxicity screening indicated that PS127-family molecules were likely to be active, 14 molecules were chosen to represent the chemical space of the PS127 family. Concentration testing was performed to ensure that molecules exhibited dose dependent cytotoxicity and a CC_{50} value (the concentration that would induce 50% cytotoxicity in MOLM-13 cells) was calculated for each compound. Twelve molecules out of the 14 PS127-molecules displayed CC_{50} under 8 µM, with four molecules (PS127_4, PS127_9, PS127_10, and PS127E) displaying a sub-micromolar CC_{50} (**Table 1**). To evaluate whether this cytotoxicity was specific for leukemic cells, CC_{50} values were also determined for healthy peripheral mononuclear blood cells (PBMCs). Each of the compounds showed at least a two-fold difference between their CC_{50} values in MOLM-13 and PBMCs, with our top four hits having over a 15-fold difference, emphasizing their selectivity.

Previous research indicated that PS127 (the founding member of the compound family) was likely to function through stimulation of autophagic recycling of mitochondria (23). For this reason, we considered the possibility that these compounds may exhibit greater toxicity to cells with increased mitochondrial dependence, such as cardiomyocytes (42). CC_{50} values of PS127-family compounds with sub-micromolar CC_{50} in MOLM-13 were calculated for the cardiomyocyte H9C2 cell line, and were determined to be ~9.5-30-fold higher than in AML cells, suggesting that mitochondrial targeting in leukemia cells was specific.

These compounds were also evaluated in a panel of other AML cell lines: MOLM-14, MV4;11, THP-1, and OCI-AML2 (**Table 2**) with a variety of genetic lesions that are frequently found in AML patients**.** Each of the prioritized PS127-molecules was active against other AML cell lines, a result crucial for targeting the heterogenous nature of AML. Based on their strong activity and low CC_{50}, PS127_4, PS127_10, and PS127E were selected for further evaluation.

PS127-family compounds are synergistic with current commercial chemotherapeutics

The rise of drug resistance in AML is a well-known phenomenon that complicates treatment in most, if not all, patient populations. Consequently, few modern chemotherapeutics are given as monotherapies. Instead, they are provided in combinations. The synergistic potential of our top compounds was tested in combination with commonly used AML chemotherapeutics. Synergy is considered to be a greater-than-additive effect when multiple treatments are combined (43).

For this purpose, PS127-family compounds were tested for synergy with the first-line treatments doxorubicin (DOX) and arabinose-C/cytarabine (ara-C) (44–46) and with midostaurin (MID), a targeted therapy used in AML patients with FLT-3 mutations (16,47). Synergy was evaluated by assessing cell viability after single and combinatorial treatments with the PS127-family compounds and AML treatments. A Bliss model was used to calculate synergy, with a score above 10 considered to indicate synergy (43). The prioritized candidates, PS127_4, PS127_10, and PS127E showed some synergy with DOX and ara-C but had the strongest synergy with MID in MOLM-13 (**Figure 2, S3, S4, S5)**. This was promising, as MOLM-13 harbors an internal tandem duplication of FLT3 (FLT3-ITD) mutation, which is the expected target of MID. Higher levels of synergy are often correlated with distinct mechanisms of action for the drugs, suggesting

that the prioritized compounds use a different mechanism compared to MID, possibly different from DOX and ara-C as well.

We also evaluated the synergistic potential of these compounds in healthy PBMCs under the same conditions. In these cells, no synergistic activity was observed between PS127-compounds and AML treatments, including MID (**Figure 2B, D and S3, S4, S5)**. Notably, there was also a concomitant difference in sensitivity: the survival of AML cells in the presence of drug combinations resulting in maximum synergy was significantly lower than in PBMCs **(Figure 2C, E**). Specifically, PBMC survival was over 85% for all combinations tested. This result reinforced the conclusion that the cytotoxicity of the drug combination was specific to leukemic cells and was unlikely to have overt side effects on healthy cells.

Since PS127-family compounds showed the highest synergy with MID, we evaluated these combinations in two additional AML cell lines: MV4;11 and OCI-AML2. MV4;11, like MOLM-13, carries an FLT3-ITD mutation, while OCI-AML2 does not contain any FLT3 mutations but still maintains high, detectable amounts of FLT3 (48). The top PS127-compounds showed high synergy with MID in MV4;11 (**Figure 3A, S6**). The combination of PS127_4 and MID produced the strongest synergy, with the Bliss score being above 60 (**Figure 3B and C**). In contrast, the combination did not significantly affect PBMC cell viability (**Figure 3B and C**). The difference in combined treatment survival between MV4;11 and PBMCs was ~10 fold (9.20% vs 93.65%). Intriguingly, prioritized PS127-compounds displayed a range of synergy with MID in OCI-AML2, despite the lack of FLT3 mutation in this cell line (**Figure 3A, Figure S7**). MID is also known to target S6 phosphorylation and sphingosine kinase-1, which likely contributes to its effective interaction with PS127-family compounds in OCI-AML2 cells (48,49). Importantly, while PS127E had comparable synergy with MID in MV4;11 and OCI-AML2, synergy scores for

PS127_4 and 127_10 were about two times lower in the latter cell line, indicating complex relationships between compound effects and cancer genotype.

In vitro validation of PASS activity predictions

To elucidate the mechanisms used by the prioritized compounds to selectively induce leukemic cell death, we began by verifying the PASS-predicted activities used for screening: apoptotic agonism, T/GRi, and autophagic induction. First, flow cytometry experiments were performed using annexin V-FITC/PI/Hoechst staining to evaluate compounds' ability to induce apoptosis. Annexin V is a protein that binds to phosphatidylserine which will be exposed during apoptosis (50). Hoechst 33342 and PI were also used to distinguish between viable and non-viable cells. MOLM-13 cells were treated with PS127E for 24 hours. Flow cytometry analysis demonstrated that PS127E significantly induced apoptosis in leukemic cells, as indicated by annexin V-positive staining (**Figure 4A**). Treatment with PS127_4 or PS127_10 also increased apoptotic activation (**Figure 4B**). Most cells killed by PS127-family compounds were positive for annexin V staining, suggesting that the primary mechanism of cytotoxicity was apoptotic activation.

Next, the ability of PS127-family compounds to induce autophagy was measured. MOLM-13 cells were treated with PS127-family molecules for 24 hours in the presence or absence of the autophagic inhibitor 3-methyladenine (3-MA) (38). The combination of 3-MA and PS127-family molecules resulted in substantial antagonism (**Figure 4C, S8A**). This antagonism restored cell viability, suggesting that functional autophagy was required for PS127-induced cytotoxicity.

Finally, the predicted inhibitory effect of PS127-family molecules on enzymes responsible for redox metabolism, specifically thioredoxin reductase (TrxR) or glutathione reductase (GSR), was evaluated. Colorimetric assays were used to assess the impact of compound on each pathway.

None of the top PS127-compounds had a significant effect on the activity of TrxR in MOLM-13 (**Figure 4D**), suggesting that none of them interacted with TrxR and that this was not the mechanism used by the compounds. Next, changes in the ratio of GSH to GSSG in the presence of these compounds were determined. Alterations to this ratio serve as an indicator that the compounds are disrupting GSR activity, as this enzyme reduces GSSG back into GSH, an antioxidant responsible for maintaining ROS homeostasis and reducing cellular oxidative stress (51,52). In contrast to what was seen for TrxR, PS127-family compounds substantially reduced the ratio of GSH to GSSG (**Figure 4D**), suggesting that they might be disrupting GSR.

PS127-compounds induce redox-dependent cytotoxicity by interfering with glutathione metabolism

The decrease in the GSH to GSSG ratio after PS127-treatment suggested further evaluation for whether other redox metabolism pathways were affected by the treatment. For this evaluation, PS127E-treated cells were supplemented with exogenous GSH, GSSG, or the GSH precursor, *N*-acetyl-cysteine (NAC). GSH and NAC completely rescued viability of PS127E-treated cells (**Figure 5A**). In contrast, supplementation with GSSG did not provide any rescue.

To determine whether the PS127-family was specifically targeting the glutathione pathway, cells were supplemented with other known antioxidants, which act independently of GSR. The first antioxidant tested was reduced ascorbate, which can be regenerated by GSH without affecting glutathione peroxidase (GPX1) or GSR activity (51,53). Ascorbate supplementation at the highest concentration that causes minimal cytotoxicity (**Figure S9C**) did not rescue PS127E-treated cells (**Figure 5A**). Similarly, α-tocopherol supplementation also failed to significantly improve survival of PS127E-treated cells (**Figure 5A**). α-tocopherol often scavenges peroxyl radicals and can

indirectly elevate GSH levels by increasing the levels of glutamylcysteine synthetase (γ-GCS), which catalyzes the first, rate-limiting step in GSH synthesis (54,55). These results reinforced the likelihood that PS127-family molecules specifically interfere with glutathione pathway, likely by preventing the ability of GSR to reduce GSSG. This would have the effect of increasing intracellular ROS. Cytotoxicity of PS127_4 or PS127_10 was similarly inhibited by GSH and unaffected by GSSG or α-tocopherol (**Figure S8B**).

To examine the relationship between ROS levels and cytotoxicity, we measured the change of total ROS and mitochondrial ROS using DHE and MitoSox staining, respectively, in cells treated with PS127-family-molecules. PS127-family-molecules significantly increased both total and mitochondrial ROS levels compared to negative controls, suggesting an oxidative stress-dependent cytotoxicity (**Figure 5B and C, S8**), likely due to the decrease of cellular GSH pools. Consistent with this, supplementation with GSH, but not with GSSG or α-tocopherol, decreased total and mitochondrial ROS levels to approximately basal levels in spite of treatment with PS127-family compounds (**Figure 5B and C, S8**). Combined, these data indicated that these compounds were likely to compromise the activity of GSR.

PS127-family compounds interfere with glutathione reductase

Differential scanning fluorimetry (DSF) was used to evaluate the possibility of direct interactions between GSR and PS127-family molecules. This technique measures the melting temperature of a target protein in the presence or absence of small molecules that may interact with the protein (56). A significant increase in protein melting temperature indicates interference with protein unfolding, likely due to an interaction between the enzyme and the small molecule. A known GSR inhibitor, 2-AAPA, was used as a positive control (57). As expected, 2-AAPA

456 significantly changed the melting temperature of GSR (**Figure 5D**). When incubated with active
457 PS127-family compounds (PS127_4, PS127_9, PS127_10, or PS127E), the melting temperature
458 of GSR similarly displayed a significant increase in melting temperature, suggesting enzyme-
459 compound interaction (**Figure 5D**). In contrast, an inactive PS127-compound analog (PS127H)
460 did not significantly change the melting temperature of GSR (**Figure 5D**). These data suggested
461 that active PS127-family molecules bind to GSR, preventing its ability to reduce GSSG and
462 reducing cellular GSH pools. Consequently, this increased cellular ROS and triggered apoptosis.
463
464 **A non-PS127-family compound, 125_1, shares PS127-family compounds' properties**
465 As described above, compounds predicted to have high probability of apoptotic agonism,
466 T/GRi, and autophagic induction are likely to be cytotoxic to AML cells. This prediction is
467 structurally agnostic, so other compounds with all three activities are also likely to have this
468 activity. Toward that end, compound 125_1, which was structurally unrelated to PS127-family but
469 was predicted to have all three activities, was chosen for further analysis. Compound 125_1
470 exhibited a low CC_{50} at 1.14 ± 0.16 μM in MOLM-13, unlike in PBMCs (6.52 ± 0.77 μM) or
471 cardiomyocytes (> 16 μM). To determine whether 125_1 uses similar mechanisms as PS127-
472 family molecules, we examined the predicted PASS activities. Annexin V-FITC/Hoescht/PI
473 staining indicated that 125_1 induced apoptotic cell death (**Figure 6A**). Moreover, 125_1 showed
474 strong antagonism with 3-MA, suggesting autophagy-dependent cytotoxicity (**Figure 6B**). Finally,
475 cells treated with 125_1 were supplemented with GSH, GSSG, or α-tocopherol. GSH significantly
476 reduced cytotoxicity, while GSSG and α-tocopherol did not (**Figure 6C**). Compound 125_1 also
477 triggered similar patterns of increased total and mitochondrial ROS levels to PS127-family
478 molecules, with GSH significantly decreasing these ROS levels (**Figure 6D and E**). Finally,

compound 125_1 also increased GSR melting temperature, indicating that this compound also binds to the enzyme (**Figure 6F**). Interestingly, 125_1 also showed synergy with MID in MOLM-13, like PS127-family molecules (**Figure 6G**). Overall, 125_1 shared the same mechanistic properties of the other compounds identified *in silico,* despite the structural dissimilarities.

Prioritized PS127-family compounds interfere with mitochondrial bioenergetics

As noted above, PS127-family compounds compromised redox homeostasis and increased mitochondrial ROS. This suggested that the compounds may be compromising mitochondrial pathways, particularly respiration. Previous reports have shown that AML cells, especially LSCs, heavily rely on OXPHOS to support the demand for ATP due to low coupling efficiency (23,58,59). We have previously reported that other compounds with selective cytotoxicity toward AML cells impair AML cell respiration and ATP production (23).

Routine respiration was measured in live AML cells after 3 hours of exposure to PS127-family compounds. As anticipated, treatment with PS127_4, PS127_10, or PS127E impaired routine respiration, indicated by reduction of oxygen consumption rate (**Figure 7A**). Similarly, compound 125_1 also significantly impaired routine respiration compared to solvent control. Importantly, this effect was independent of cell death as more than 85% cells were alive at this time point.

Finally, ATP production was measured after 3 hours of exposure to these GSR inhibitors using a commercial assay. In line with previous result (23), PS127_4, PS127_10, PS127E, and 125_1 significantly decreased ATP production (**Figure 7B**). Similarly to routine respiration, this effect was independent of cell death as more than 95% cells were alive at the time of cell lysis to measure ATP levels.

DISCUSSION

It remains critically important to identify new, improved treatments for AML that decrease the risk of relapse and have better potential for patient populations who cannot tolerate standard induction and consolidation regimens, including elderly or those with serious co-morbidities. Targeting dysfunctional mitochondria present in leukemic blast and stem cells is one increasingly promising approach. One of the key obstacles in drug discovery is finding small molecules that demonstrate appropriate selectivity for diseased cells compared to their healthy counterparts, a ratio known as the therapeutic window.

In order to more efficiently probe chemical space and more effectively identify promising leads, researchers have begun to leverage *in silico* techniques like ligand- and structure-based screening methods (60)**.** These methods have been extensively reviewed, but they are undergoing constant evolution with the integration of AI approaches. For example, some of the more popular approaches of computer-aided drug design include quantitative structure-activity relationship (qSAR) assays, molecular docking, and pharmacophore modeling (61). Structure-based screen methods are promising but they are limited to known structures, often taken from X-ray, cryo-EM, or NMR structures. If no structure is available, researchers are forced to rely on predicted structures gained from homology modeling or template-free, AI predictions like AlphaFold. These techniques, while powerful, require considerable data input and computing power. Ligand-based drug design approaches like qSAR or acquisition of virtual libraries followed by molecular docking are other common approaches, but they suffer from the same problems (62,63). When looking for more approachable cheminformatic methods, function-based methods like PASS are appealing. PASS is a ligand-based cheminformatic approach that has been trained on structural-activity relationships of thousands of known bioactive compounds, which enables a function-based

in silico screen. PASS can rapidly predict the biological functions of millions of unknown molecules, enabling a search for specific functions (64,65). The approaches are not mutually exclusive; researchers have begun to integrate PASS software as an input into qSAR to obtain independent model outputs (66).

Using PASS, we identified potential biochemical functions for the previously identified PS127-family compounds (23). Compounds were predicted to have apoptotic agonism and T/GRi activity. Active compounds triggered cell death in AML blasts and stem cells by inducing depolarization of the mitochondrial membrane, upregulating ROS, and decreasing routine and ATP-linked respiration. At the same time, the active compounds did not significantly induce changes in healthy PBMCs, indicating their selectivity. We were interested in employing function-based cheminformatics to identify additional small molecules with these properties, so we integrated PASS into our *in silico* pipeline to identify additional hits that may share those activities. Using this approach, we tested a wide chemical space without employing large computational resources, like qSAR and exploratory molecular docking.

Using this approach, 161 hits were obtained, 82 of which structurally clustered with known PS127-family molecules. In total, 14 selected *in silico* hits were examined *in vitro*, 12 of which were active. Meanwhile, all 4 compounds tested from the second largest group, cluster 103, were inactive. To understand the relevant difference between the activity of these two groups, we analyzed additional predicted PASS activities using an extended version of the software. This revealed a third activity, autophagic induction, that was predicted to be present in PS127-family compounds but absent from cluster 103 molecules. This function was consistent, as the parent PS127 molecule was identified in a screen for mitophagic activators. Since PS127-family

molecules affected mitochondrial function, we hypothesized that this activity could be relevant to AML cell cytotoxicity.

We filtered our 161 hits to remove those without autophagic induction activity, which reduced the number of total molecules to 93. Notably, this cut only a single molecule from the PS127-family group. To determine whether the three functions together were sufficient to discriminate between active and inactive compounds, five of the 12 non-PS127-family molecules remaining were ordered and tested for cytotoxic activity. Most showed strong cytotoxic potential.

Our study highlights the value of function-based selection in discovering novel bioactive compounds. PASS also revealed a more complete characterization of the chemical space for PS127-family molecules before *in vitro* testing began. PS127-family molecules were originally predicted to promote cell death and interfere with redox homeostasis, and based on previous *C. elegans* data, we predicted they also initiate mitophagy (23). The predicted functions of the molecules were reasonably connected as changes in redox homeostasis, particularly oxidative stress, have been linked to mitophagic induction (67). Additionally, the partially dysfunctional mitochondria present in AML cells allow PS127-family compounds to tip the ROS balance toward initiation of mitophagy in leukemic cells, while healthy cells are able to utilize their normal mechanisms to maintain homeostasis (18,67–69).

We also evaluated whether our compounds synergize with current AML treatments, as the therapeutic regimen often involves multiple drugs being administered at once. The first-line treatment of AML includes induction followed by consolidation. Induction de-bulks the leukemic mass by inducing profound cell death in the proliferated leukemic blasts residing in the bone marrow and blood. Most commonly provided in a “7 + 3” treatment plan, induction involves the administration of high dose ara-C for seven days to disrupt DNA replication in combination with

an anthracycline (e.g. doxorubicin, daunorubicin, or idarubicin) for the first three days (70). To reduce relapse, induction is followed up by consolidation, a post-remission plan involving ongoing, high-dose of ara-C treatment often with targeted therapeutics to further decrease and maintain low blast numbers. Therefore, we tested for synergy between DOX or ara-C and our PS127-family compounds. We also included a tyrosine kinase receptor inhibitor, MID, which is often administered during induction and consolidation to AML patients with FLT-3 mutations, which accounts for about 30% of the patient population (71). Interestingly, MID has also been found to be effective *in vitro* against AML cells lines without FLT-3 mutations, like OCI-AML2 (48). MV4;11, a cell line with an FLT3-ITD mutation, showed the highest synergy with PS127-family molecules, with scores for PS127_4/MID averaging over 60. This suggests that patients with genotypes similar to MV4;11 may benefit from this treatment combination. In contrast, PS127E/MID showed higher synergy in OCI-AML2 cells.

While our compounds were also synergistic with DOX, the magnitude was lower. This reduced synergistic potential may be due to the cascade of effects that result from inhibiting DNA replication, including interfering with mitochondrial bioenergetics and respiration, leading to some mechanistic overlap with the PS127-compounds (72). However, DOX has also been linked to cardiotoxicity via mitochondrial targeting (72). This suggests that PS127-family compounds, which did not show cardiotoxicity at concentrations that killed AML cells, may be useful as an alternative. Additionally, synergy is important when treating patient populations that are sensitive to high chemotherapeutic dosing or when the risk of relapse is high. Some studies show that drug combinations may promote resistance, but monotherapy is not often strong enough to induce remission in patients (68,73,74). Ultimately, patients would need to be evaluated on a case-by-case basis to determine whether intensive induction and consolidation should be the first step, and

593 which mutation-specific drugs should be administered (75). While some researchers are looking
594 into pre-approved FDA drugs for other diseases to add to the arsenal of drugs to treat sensitive and
595 high-risk patients, our goal was to find novel chemotherapeutics and uncover their mechanisms of
596 action (76).

597 AML cells, particularly LSCs, have been found to be "addicted" to glutathione, diverging from
598 the traditional Warburg metabolism that assumes leukemic cells upregulate glycolysis, and rely on
599 the sensitive balance of mitophagy for cell survival and proliferation (21,77). LSCs are thought to
600 be one cause of relapse in AML patients, the other likely being acquired resistance in myeloblasts
601 (78–80). Relapse is often attributed to LSCs as their slow division makes them less susceptible to
602 the anti-proliferative chemotherapeutics used in first-line treatment, like anthracyclines (81,82).
603 By targeting both blasts and LSCs metabolism, patients will have a higher chance of remaining in
604 complete remission. These PS127-family compounds interfere with the glutathione redox balance,
605 almost definitely by inhibiting GSR. Previously, we showed that PS127B and PS127E activate
606 high levels of apoptosis in LSCs but not healthy hematopoietic stem cells (23). This is consistent
607 with literature reports on GSR targeting being effective in eliminating LSCs (21,83).

608 Targeting redox homeostasis has become increasingly appealing as an approach to treat
609 heterogenous populations like AML. One of the most recently approved AML chemotherapeutics
610 is a BCL-2 inhibitor. BCL-2 is a regulator of mitochondrial respiration, therefore inhibitors like
611 ABT-737 and ABT-263 are able to selectively induce cell death in leukemic cells with low ROS
612 levels while not affecting PBMCs health (82). Venetoclax became the first approved BCL-2
613 inhibitor for newly diagnosed, sensitive AML patient populations (75,84,85). Redox homeostasis
614 can also be altered indirectly. For example, first line chemotherapeutics like DOX and ara-C that
615 have downstream effects that decrease the GSH to GSSG ratio in different subcellular components

of AML cells, despite DNA replication being each drug's primary target (86). Previous research by others showed that inhibiting GSR or TrxR, particularly TrxR1, may be effective for cancer therapy (21,87,88). The thioredoxin and glutathione systems are the two most important routes for ROS detoxification in eukaryotes (89).

We used a structure-blind, function-based cheminformatic approach to identify compounds that selectively kill AML cells and provide a foundation to uncovering target pathway and protein for these molecules. We validated their predicted functions, including inhibition of glutathione metabolism, likely via interfering with the function of GSR. High synergy with MID underscores therapeutic promise of these molecules and validates our approach. Our preliminary evidence suggests that these compounds have a large therapeutic window and show genotype-specific effects. Although these compounds show considerable promise, there are still important questions. For example, compound pharmacokinetics are an important consideration when evaluating new potential drugs for clinical application. Additionally, evaluation of these compounds in patient-derived cells will also provide critical data about their clinical potential. These are key questions for which we are enthusiastically searching for answers.

ACKNOWLEDGEMENTS

This research was supported by NIH NIGMS (R35GM129294) and NCI (R21CA280500) grants to NVK, and an NIGMS (T32GM139801) grant to MRD. DSF guidance was provided by Dr. Katelyn Baumer (Rice University). *In silico* analysis was performed within the framework of the Program for Basic Research in the Russian Federation for a long-time period (2021-2030) (project 122030100170-5 awarded to VVP).

AUTHOR CONTRIBUTIONS

MRD and BM performed the majority of the experiments, performed data analysis and visualization, generated all the figures, and drafted and edited the manuscript. ET and AVR helped with the initial *in silico* screen and some preliminary experiments. LAS and VVP performed *in silico* analysis. SRG participated in selecting the molecules from the *in silico* screen and provided a medical chemist's perspective on molecule activity. NVK provided overall funding, and crucial support and guidance for this study. NVK also contributed to data analysis, experimental design, and manuscript writing and editing. All authors reviewed the manuscript before submission.

COMPETING INTERESTS

The authors declare no competing interests.

REFERENCES

1. Tober R, Schnetzke U, Fleischmann M, Yomade O, Schrenk K, Hammersen J, et al. Impact of treatment intensity on infectious complications in patients with acute myeloid leukemia. J Cancer Res Clin Oncol. 2023 Apr;149(4):1569–83. https://doi.org/10.1007/s00432-022-03995-2

2. Blum W, Matthews V. Fast Facts: Acute myeloid leukemia. Karger; 2018.

3. Zhang J, Gu Y, Chen B. Mechanisms of drug resistance in acute myeloid leukemia. OncoTargets Ther. 2019 Mar;Volume 12:1937–45. https://doi.org/10.2147/OTT.S191621

4. Nasr R, Lorendeau D, Khonkarn R, Dury L, Pérès B, Boumendjel A, et al. Molecular analysis of the massive GSH transport mechanism mediated by the human Multidrug Resistant Protein 1/ABCC1. Sci Rep. 2020 May 6;10(1):7616. https://doi.org/10.1038/s41598-020-64400-x

5. Lorendeau D, Dury L, Nasr R, Boumendjel A, Teodori E, Gutschow M, et al. MRP1-dependent Collateral Sensitivity of Multidrug-resistant Cancer Cells: Identifying Selective Modulators Inducing Cellular Glutathione Depletion. Curr Med Chem. 2017;24(12):1186–213. https://doi.org/10.2174/0929867324666161118130238 PMID: 27855620

6. Chial H. Proto-oncogenes to Oncogenes to Cancer [Internet]. Nature Education. https://www.nature.com/scitable/topicpage/proto-oncogenes-to-oncogenes-to-cancer-883/

7. Dany M, Gencer S, Nganga R, Thomas RJ, Oleinik N, Baron KD, et al. Targeting FLT3-ITD signaling mediates ceramide-dependent mitophagy and attenuates drug resistance in AML. Blood. 2016 Oct 13;128(15):1944–58. https://doi.org/10.1182/blood-2016-04-708750 PMID: 27540013

8. Larrosa-Garcia M, Baer MR. FLT3 inhibitors in acute myeloid leukemia: Current status and future directions. Mol Cancer Ther. 2017 Jun;16(6):991. https://doi.org/10.1158/1535-7163.MCT-16-0876 PMID: 28576946

9. Perl AE, Altman JK, Cortes J, Smith C, Litzow M, Baer MR, et al. Selective Inhibition of FLT3 by Gilteritinib in Relapsed/Refractory Acute Myeloid Leukemia: a Multicenter, First-in-human, Open-label, Phase 1/2 Study. Lancet Oncol. 2017 Jun 20;18(8):1061. https://doi.org/10.1016/S1470-2045(17)30416-3 PMID: 28645776

10. Smith CC, Wang Q, Chin C-S, Salerno S, Damon LE, Levis MJ, et al. Validation of ITD mutations in FLT3 as a therapeutic target in human acute myeloid leukaemia. Nature. 2012 May;485(7397):260–3. https://doi.org/10.1038/nature11016

11. Zhao JC, Agarwal S, Ahmad H, Amin K, Bewersdorf JP, Zeidan AM. A review of FLT3 inhibitors in acute myeloid leukemia. Blood Rev. 2022 Mar;52:100905. https://doi.org/10.1016/j.blre.2021.100905 PMID: 34774343

12. Sierra J, Montesinos P, Thomas X, Griskevicius L, Cluzeau T, Caillot D, et al. Midostaurin plus daunorubicin or idarubicin for young and older adults with FLT3-mutated AML: a phase 3b trial. Blood Adv. 2023 Aug 17;7(21):6441. https://doi.org/10.1182/bloodadvances.2023009847 PMID: 37581981

13. Chen X, Glytsou C, Zhou H, Narang S, Reyna DE, Lopez A, et al. Targeting Mitochondrial Structure Sensitizes Acute Myeloid Leukemia to Venetoclax Treatment. Cancer Discov. 2019 Jul 1;9(7):890–909. https://doi.org/10.1158/2159-8290.CD-19-0117

14. Burchert A, Bug G, Fritz LV, Finke J, Stelljes M, Röllig C, et al. Sorafenib Maintenance After Allogeneic Hematopoietic Stem Cell Transplantation for Acute Myeloid Leukemia With *FLT3* –Internal Tandem Duplication Mutation (SORMAIN). J Clin Oncol. 2020 Sep 10;38(26):2993–3002. https://doi.org/10.1200/JCO.19.03345

15. Griffin JD, Song Y, Yang H, Freimark J, Shah MV. Post-transplant maintenance therapy in patients with FLT3-mutated acute myeloid leukemia: Real-world treatment patterns and outcomes. Eur J Haematol. 2021 Aug 11;107(5):553. https://doi.org/10.1111/ejh.13692 PMID: 34289175

16. Stone RM, Mandrekar SJ, Sanford BL, Laumann K, Geyer S, Bloomfield CD, et al. Midostaurin plus Chemotherapy for Acute Myeloid Leukemia with a FLT3 Mutation. N Engl J Med. 2017 Aug 3;377(5):454–64. https://doi.org/10.1056/NEJMoa1614359

17. Panina SB, Pei J, Kirienko NV. Mitochondrial metabolism as a target for acute myeloid leukemia treatment. Cancer Metab. 2021 Dec;9(1):17. https://doi.org/10.1186/s40170-021-00253-w

18. Tjahjono E, Daneman MR, Meika B, Revtovich AV, Kirienko NV. Mitochondrial abnormalities as a target of intervention in acute myeloid leukemia. Front Oncol. 2025 Jan 20;14:1532857. https://doi.org/10.3389/fonc.2024.1532857

19. Mesbahi Y, Trahair TN, Lock RB, Connerty P. Exploring the Metabolic Landscape of AML: From Haematopoietic Stem Cells to Myeloblasts and Leukaemic Stem Cells. Front Oncol. 2022 Feb 10;12:807266. https://doi.org/10.3389/fonc.2022.807266

20. Feng L, Zhang PY, Gao W, Yu J, Robson SC. Targeting chemoresistance and mitochondria-dependent metabolic reprogramming in acute myeloid leukemia. Front Oncol. 2023 Sep 7;13:1244280. https://doi.org/10.3389/fonc.2023.1244280

21. Pei S, Minhajuddin M, Callahan KP, Balys M, Ashton JM, Neering SJ, et al. Targeting Aberrant Glutathione Metabolism to Eradicate Human Acute Myelogenous Leukemia Cells. J Biol Chem. 2013 Nov 22;288(47):33542–58. https://doi.org/10.1074/jbc.M113.511170 PMID: 24089526

22. Baccelli I, Gareau Y, Lehnertz B, Gingras S, Spinella J-F, Corneau S, et al. Mubritinib Targets the Electron Transport Chain Complex I and Reveals the Landscape of OXPHOS Dependency in Acute Myeloid Leukemia. Cancer Cell. 2019 Jul 8;36(1):84-99.e8. https://doi.org/10.1016/j.ccell.2019.06.003 PMID: 31287994

23. Panina SB, Pei J, Baran N, Tjahjono E, Patel S, Alatrash G, et al. Novel mitochondria-targeting compounds selectively kill human leukemia cells. Leukemia. 2022 Aug;36(8):2009–21. https://doi.org/10.1038/s41375-022-01614-0

24. Catalano G, Zaza A, Banella C, Pelosi E, Castelli G, de Marinis E, et al. MCL1 regulates AML cells metabolism via direct interaction with HK2. Metabolic signature at onset predicts overall survival in AMLs' patients. Leukemia. 2023 Aug;37(8):1600–10. https://doi.org/10.1038/s41375-023-01946-5

25. Fay HRS, Dykstra KM, Johnson M, Cronin TL, Lutgen-Dunckley L, Martens BL, et al. Mitophagy Plays a Key Role in the Anti-Leukemic Activity of Autophagy Inhibitors Under Hypoxia in Acute Myeloid Leukemia. Blood. 2019 Nov 13;134(Supplement_1):1278–1278. https://doi.org/10.1182/blood-2019-127024

26. Dykstra KM, Fay HRS, Massey AC, Yang N, Johnson M, Portwood S, et al. Inhibiting autophagy targets human leukemic stem cells and hypoxic AML blasts by disrupting

738 mitochondrial homeostasis. Blood Adv. 2021 Apr 27;5(8):2087–100.
739 https://doi.org/10.1182/bloodadvances.2020002666 PMID: 33877295

740 27. Morad SAF, Ryan TE, Neufer PD, Zeczycki TN, Davis TS, MacDougall MR, et al. Ceramide-
741 tamoxifen regimen targets bioenergetic elements in acute myelogenous leukemia1. J Lipid
742 Res. 2016 Jul;57(7):1231–42. https://doi.org/10.1194/jlr.M067389 PMID: 27140664

743 28. Glytsou C, Chen X, Zacharioudakis E, Al-Santli W, Zhou H, Nadorp B, et al. Mitophagy
744 Promotes Resistance to BH3 Mimetics in Acute Myeloid Leukemia. Cancer Discov. 2023 Jul
745 7;13(7):1656–77. https://doi.org/10.1158/2159-8290.CD-22-0601 PMID: 37088914

746 29. Salwa A, Ferraresi A, Vallino L, Maheshwari C, Moia R, Gaidano G, et al. High Mitophagy
747 and Low Glycolysis Predict Better Clinical Outcomes in Acute Myeloid Leukemias. Int J Mol
748 Sci. 2024 Oct 27;25(21):11527. https://doi.org/10.3390/ijms252111527 PMID: 39519080

749 30. Panina SB, Baran N, Brasil Da Costa FH, Konopleva M, Kirienko NV. A mechanism for
750 increased sensitivity of acute myeloid leukemia to mitotoxic drugs. Cell Death Dis. 2019
751 Aug 13;10(8):617. https://doi.org/10.1038/s41419-019-1851-3

752 31. Panina SB, Pei J, Baran N, Konopleva M, Kirienko NV. Utilizing Synergistic Potential of
753 Mitochondria-Targeting Drugs for Leukemia Therapy. Front Oncol. 2020 Apr 3;10:435.
754 https://doi.org/10.3389/fonc.2020.00435

755 32. Tjahjono E, Pei J, Revtovich AV, Liu T-JE, Swadi A, Hancu MC, et al. Mitochondria-affecting
756 small molecules ameliorate proteostasis defects associated with neurodegenerative
757 diseases. Sci Rep. 2021 Sep 6;11(1):17733. https://doi.org/10.1038/s41598-021-97148-z

758 33. Lagunin A, Stepanchikova A, Filimonov D, Poroikov V. PASS: prediction of activity spectra
759 for biologically active substances. Bioinforma Oxf Engl. 2000 Aug;16(8):747–8.
760 https://doi.org/10.1093/bioinformatics/16.8.747 PMID: 11099264

761 34. Backman TWH, Cao Y, Girke T. ChemMine tools: an online service for analyzing and
762 clustering small molecules. Nucleic Acids Res. 2011 Jul;39(Web Server issue):W486-491.
763 https://doi.org/10.1093/nar/gkr320 PMID: 21576229

764 35. Pei J, Panina SB, Kirienko NV. An automated differential nuclear staining assay for accurate
765 determination of mitocan cytotoxicity. J Vis Exp JoVE. 2020 May 12;(159):10.3791/61295.
766 https://doi.org/10.3791/61295 PMID: 32478749

767 36. Ritz C, Baty F, Streibig JC, Gerhard D. Dose-Response Analysis Using R. PLOS ONE. 2015 Dec
768 30;10(12):e0146021. https://doi.org/10.1371/journal.pone.0146021

769 37. Ianevski A, Giri AK, Aittokallio T. SynergyFinder 3.0: an interactive analysis and consensus
770 interpretation of multi-drug synergies across multiple samples. Nucleic Acids Res. 2022 Jul
771 5;50(W1):W739–43. https://doi.org/10.1093/nar/gkac382 PMID: 35580060

38. Heckmann BL, Yang X, Zhang X, Liu J. The autophagic inhibitor 3-methyladenine potently stimulates PKA-dependent lipolysis in adipocytes. Br J Pharmacol. 2013 Jan;168(1):163–71. https://doi.org/10.1111/j.1476-5381.2012.02110.x PMID: 22817685

39. Wu T, Hornsby M, Zhu L, Yu JC, Shokat KM, Gestwicki JE. Protocol for performing and optimizing differential scanning fluorimetry experiments. STAR Protoc. 2023 Dec;4(4):102688. https://doi.org/10.1016/j.xpro.2023.102688

40. Wu T, Gale-Day ZJ, Gestwicki JE. DSFworld: A flexible and precise tool to analyze differential scanning fluorimetry data. Protein Sci Publ Protein Soc. 2024 Jun;33(6):e5022. https://doi.org/10.1002/pro.5022 PMID: 38747440

41. Filimonov DA, Lagunin AA, Gloriozova TA, Rudik AV, Druzhilovskii DS, Pogodin PV, et al. Prediction of the Biological Activity Spectra of Organic Compounds Using the Pass Online Web Resource. Chem Heterocycl Compd. 2014 Jun 1;50(3):444–57. https://doi.org/10.1007/s10593-014-1496-1

42. Picca A, Mankowski RT, Burman JL, Donisi L, Kim J-S, Marzetti E, et al. Mitochondrial quality control mechanisms as molecular targets in cardiac ageing. Nat Rev Cardiol. 2018 Sep;15(9):543–54. https://doi.org/10.1038/s41569-018-0059-z PMID: 30042431

43. Ianevski A, Giri AK, Aittokallio T. SynergyFinder 2.0: visual analytics of multi-drug combination synergies. Nucleic Acids Res. 2020 Jul 2;48(W1):W488–93. https://doi.org/10.1093/nar/gkaa216 PMID: 32246720

44. Liu H. Emerging agents and regimens for AML. J Hematol OncolJ Hematol Oncol. 2021 Mar 23;14:49. https://doi.org/10.1186/s13045-021-01062-w PMID: 33757574

45. Rai KR, Holland JF, Glidewell OJ, Weinberg V, Brunner K, Obrecht JP, et al. Treatment of acute myelocytic leukemia: a study by cancer and leukemia group B. Blood. 1981 Dec;58(6):1203–12. https://doi.org/10.1182/blood.V58.6.1203.1203 PMID: 6946847

46. Fernandez HF, Sun Z, Yao X, Litzow MR, Luger SM, Paietta EM, et al. Anthracycline Dose Intensification in Acute Myeloid Leukemia. N Engl J Med. 2009 Sep 24;361(13):1249–59. https://doi.org/10.1056/NEJMoa0904544

47. Gallogly MM, Lazarus HM, Cooper BW. Midostaurin: a novel therapeutic agent for patients with FLT3-mutated acute myeloid leukemia and systemic mastocytosis. Ther Adv Hematol. 2017 Sep;8(9):245–61. https://doi.org/10.1177/2040620717721459 PMID: 29051803

48. Weisberg E, Meng C, Case AE, Tiv HL, Gokhale PC, Buhrlage SJ, et al. Effects of the multi-kinase inhibitor midostaurin in combination with chemotherapy in models of acute myeloid leukaemia. J Cell Mol Med. 2020 Mar;24(5):2968–80. https://doi.org/10.1111/jcmm.14927 PMID: 31967735

49. Şahin HN, Adan A. Combined effect of midostaurin and sphingosine kinase-1 inhibitor on FMS-like tyrosine kinase 3 (FLT3) wild type acute myeloid leukemia cells. Turk J Biochem. 2022 Feb 1;47(1):49–58. https://doi.org/10.1515/tjb-2021-0152

50. Logue SE, Elgendy M, Martin SJ. Expression, purification and use of recombinant annexin V for the detection of apoptotic cells. Nat Protoc. 2009 Sep;4(9):1383–95. https://doi.org/10.1038/nprot.2009.143

51. Foyer CH, Noctor G. Ascorbate and Glutathione: The Heart of the Redox Hub1. Plant Physiol. 2011 Jan;155(1):2–18. https://doi.org/10.1104/pp.110.167569 PMID: 21205630

52. Foyer CH, Kunert K. The ascorbate–glutathione cycle coming of age. J Exp Bot. 2024 Jan 18;75(9):2682–99. https://doi.org/10.1093/jxb/erae023 PMID: 38243395

53. Gęgotek A, Skrzydlewska E. Antioxidative and Anti-Inflammatory Activity of Ascorbic Acid. Antioxidants. 2022 Oct 7;11(10):1993. https://doi.org/10.3390/antiox11101993 PMID: 36290716

54. Masaki H, Okano Y, Ochiai Y, Obayashi K, Akamatsu H, Sakurai H. alpha-tocopherol increases the intracellular glutathione level in HaCaT keratinocytes. Free Radic Res. 2002 Jun;36(6):705–9. https://doi.org/10.1080/10715760210873 PMID: 12180196

55. Siler-Marsiglio KI, Pan Q, Paiva M, Madorsky I, Khurana NC, Heaton MB. Mitochondrially targeted vitamin E and vitamin E mitigate ethanol-mediated effects on cerebellar granule cell antioxidant defense systems. Brain Res. 2005 Aug 9;1052(2):202–11. https://doi.org/10.1016/j.brainres.2005.06.030

56. Vivoli M, Novak HR, Littlechild JA, Harmer NJ. Determination of Protein-ligand Interactions Using Differential Scanning Fluorimetry. J Vis Exp JoVE. 2014 Sep 13;(91):51809. https://doi.org/10.3791/51809 PMID: 25285605

57. de Souza LF, Schmitz AE, da Silva LCS, de Oliveira KA, Nedel CB, Tasca CI, et al. Inhibition of reductase systems by 2-AAPA modulates peroxiredoxin oxidation and mitochondrial function in A172 glioblastoma cells. Toxicol In Vitro. 2017 Aug 1;42:273–80. https://doi.org/10.1016/j.tiv.2017.04.028

58. Nelson MA, McLaughlin KL, Hagen JT, Coalson HS, Schmidt C, Kassai M, et al. Intrinsic OXPHOS limitations underlie cellular bioenergetics in leukemia. eLife. 2021 Jun 16;10:e63104. https://doi.org/10.7554/eLife.63104

59. Peng M, Huang Y, Zhang L, Zhao X, Hou Y. Targeting Mitochondrial Oxidative Phosphorylation Eradicates Acute Myeloid Leukemic Stem Cells. Front Oncol. 2022 Apr 29;12:899502. https://doi.org/10.3389/fonc.2022.899502

60. Vyas VK, Bhati S, Patel S, Ghate M. Structure- and ligand-based drug design methods for the modeling of antimalarial agents: a review of updates from 2012 onwards. J Biomol

Struct Dyn. 2022 Nov 29;40(20):10481–506. https://doi.org/10.1080/07391102.2021.1932598

61. Yang S-Y. Pharmacophore modeling and applications in drug discovery: challenges and recent advances. Drug Discov Today. 2010 Jun 1;15(11):444–50. https://doi.org/10.1016/j.drudis.2010.03.013

62. Paggi JM, Pandit A, Dror RO. The Art and Science of Molecular Docking. Annu Rev Biochem. 2024 Aug;93(1):389–410. https://doi.org/10.1146/annurev-biochem-030222-120000 PMID: 38594926

63. Vilar S, Costanzi S. Predicting Biological Activities through QSAR Analysis and Docking-based Scoring. Methods Mol Biol Clifton NJ. 2012;914:271–84. https://doi.org/10.1007/978-1-62703-023-6_16 PMID: 22976034

64. Dutra NS, da Silva D'Ávila CM, da Silva TC, de Oliveira Mendes T, Livinalli IC, Bertoncelli ACZ, et al. Biological properties of caffeine, (+)-catechin, and theobromine: an in silico study. 3 Biotech. 2024 Apr;14(4):94. https://doi.org/10.1007/s13205-024-03934-7 PMID: 38444785

65. Fatima I, Rehman A, Wang P, He Z, Liao M. Discovery of Small Molecule Inhibitors Targeting CTNNB1 (β-catenin) for Endometrial cancer: Employing 3D QSAR, Drug-Likeness Assessment, ADMET Predictions, Molecular Docking and Simulation. Curr Med Chem. 2024 Sep 23; https://doi.org/10.2174/0109298673307257240826111754 PMID: 39318004

66. Lagunin A, Zakharov A, Filimonov D, Poroikov V. QSAR Modelling of Rat Acute Toxicity on the Basis of PASS Prediction. Mol Inform. 2011;30(2–3):241–50. https://doi.org/10.1002/minf.201000151

67. Garza-Lombó C, Pappa A, Panayiotidis MI, Franco R. Redox Homeostasis, Oxidative Stress and Mitophagy. Mitochondrion. 2020 Mar;51:105–17. https://doi.org/10.1016/j.mito.2020.01.002 PMID: 31972372

68. Fan C, Yang X, Yan L, Shi Z. Oxidative stress is two-sided in the treatment of acute myeloid leukemia. Cancer Med. 2024 May 8;13(9):e6806. https://doi.org/10.1002/cam4.6806 PMID: 38715546

69. Rodriguez-Zabala M, Ramakrishnan R, Reinbach K, Ghosh S, Oburoglu L, Falqués-Costa A, et al. Combined GLUT1 and OXPHOS inhibition eliminates acute myeloid leukemia cells by restraining their metabolic plasticity. Blood Adv. 2023 Sep 26;7(18):5382–95. https://doi.org/10.1182/bloodadvances.2023009967 PMID: 37505194

70. Frisch A, Rowe JM, Ofran Y. The increasingly blurred line between induction, consolidation and maintenance in acute myeloid leukaemia. Br J Haematol. 2023 Mar;200(5):556–62. https://doi.org/10.1111/bjh.18613

71. Kiyoi H, Kawashima N, Ishikawa Y. FLT3 mutations in acute myeloid leukemia: Therapeutic paradigm beyond inhibitor development. Cancer Sci. 2020 Feb;111(2):312–22. https://doi.org/10.1111/cas.14274 PMID: 31821677

72. Wu BB, Leung KT, Poon EN-Y. Mitochondrial-Targeted Therapy for Doxorubicin-Induced Cardiotoxicity. Int J Mol Sci. 2022 Feb 9;23(3):1912. https://doi.org/10.3390/ijms23031912 PMID: 35163838

73. DiNardo CD, Pratz K, Pullarkat V, Jonas BA, Arellano M, Becker PS, et al. Venetoclax combined with decitabine or azacitidine in treatment-naive, elderly patients with acute myeloid leukemia. Blood. 2019 Jan 3;133(1):7–17. https://doi.org/10.1182/blood-2018-08-868752

74. Mason-Osann E, Pomeroy AE, Palmer AC, Mettetal JT. Synergistic Drug Combinations Promote the Development of Resistance in Acute Myeloid Leukemia. Blood Cancer Discov. 2024 Mar 1;5(2):95–105. https://doi.org/10.1158/2643-3230.BCD-23-0067 PMID: 38232314

75. Kantarjian HM, DiNardo CD, Kadia TM, Daver NG, Altman JK, Stein EM, et al. Acute myeloid leukemia management and research in 2025. Ca. 2025;75(1):46–67. https://doi.org/10.3322/caac.21873 PMID: 39656142

76. Karsa M, Kosciolek A, Bongers A, Mariana A, Failes T, Gifford AJ, et al. Exploiting the reactive oxygen species imbalance in high-risk paediatric acute lymphoblastic leukaemia through auranofin. Br J Cancer. 2021 Jul 6;125(1):55–64. https://doi.org/10.1038/s41416-021-01332-x PMID: 33837299

77. Pei S, Minhajuddin M, Adane B, Khan N, Stevens BM, Mack SC, et al. AMPK/FIS1-mediated mitophagy is required for self-renewal of human AML stem cells. Cell Stem Cell. 2018 Jun 14;23(1):86. https://doi.org/10.1016/j.stem.2018.05.021 PMID: 29910151

78. Pollyea DA, Jordan CT. Therapeutic targeting of acute myeloid leukemia stem cells. Blood. 2017 Mar 23;129(12):1627–35. https://doi.org/10.1182/blood-2016-10-696039

79. Olesinski EA, Bhatia KS, Wang C, Pioso MS, Lin XX, Mamdouh AM, et al. Acquired Multidrug Resistance in AML Is Caused by Low Apoptotic Priming in Relapsed Myeloblasts. Blood Cancer Discov. 2024 May 1;5(3):180–201. https://doi.org/10.1158/2643-3230.BCD-24-0001 PMID: 38442309

80. Joshi SK, Nechiporuk T, Bottomly D, Piehowski PD, Reisz JA, Pittsenbarger J, et al. The AML microenvironment catalyzes a step-wise evolution to gilteritinib resistance. Cancer Cell. 2021 Jul 12;39(7):999-1014.e8. https://doi.org/10.1016/j.ccell.2021.06.003 PMID: 34171263

81. Al-Hamaly MA, Winter E, Blackburn JS. The mitochondria as an emerging target of self-renewal in T-cell acute lymphoblastic leukemia. Cancer Biol Ther. 2025 Feb 4;26(1):2460252. https://doi.org/10.1080/15384047.2025.2460252 PMID: 39905687

82. Lagadinou ED, Sach A, Callahan K, Rossi RM, Neering SJ, Minhajuddin M, et al. BCL-2 Inhibition Targets Oxidative Phosphorylation and Selectively Eradicates Quiescent Human Leukemia Stem Cells. Cell Stem Cell. 2013 Mar 7;12(3):329–41. https://doi.org/10.1016/j.stem.2012.12.013 PMID: 23333149

83. Costa RGA, Silva SLR, Dias IRSB, Oliveira M de S, Rodrigues ACB da C, Dias RB, et al. Emerging drugs targeting cellular redox homeostasis to eliminate acute myeloid leukemia stem cells. Redox Biol. 2023 Jun;62:102692. https://doi.org/10.1016/j.redox.2023.102692 PMID: 37031536

84. Wei AH, Strickland SA, Hou J-Z, Fiedler W, Lin TL, Walter RB, et al. Venetoclax Combined With Low-Dose Cytarabine for Previously Untreated Patients With Acute Myeloid Leukemia: Results From a Phase Ib/II Study. J Clin Oncol. 2019 May 20;37(15):1277–84. https://doi.org/10.1200/JCO.18.01600

85. Wei AH, Loo S, Daver N. How I treat patients with AML using azacitidine and venetoclax. Blood. 2025 Mar 20;145(12):1237–50. https://doi.org/10.1182/blood.2024024009

86. Abbas G, Cui M, Wang D, Li M, Zhang X-E. Construction of Genetically Encoded Biosensors to Monitor Subcellular Compartment-Specific Glutathione Response to Chemotherapeutic Drugs in Acute Myeloid Leukemia Cells. Anal Chem. 2023 Jan 26;95(5):2838–47. https://doi.org/10.1021/acs.analchem.2c04255 PMID: 36701391

87. Kennedy L, Sandhu JK, Harper M-E, Cuperlovic-Culf M. Role of Glutathione in Cancer: From Mechanisms to Therapies. Biomolecules. 2020 Oct 9;10(10):1429. https://doi.org/10.3390/biom10101429 PMID: 33050144

88. Lu J, Chew E-H, Holmgren A. Targeting thioredoxin reductase is a basis for cancer therapy by arsenic trioxide. Proc Natl Acad Sci. 2007 Jul 24;104(30):12288–93. https://doi.org/10.1073/pnas.0701549104

89. Arnér ESJ. Focus on mammalian thioredoxin reductases--important selenoproteins with versatile functions. Biochim Biophys Acta. 2009 Jun;1790(6):495–526. https://doi.org/10.1016/j.bbagen.2009.01.014 PMID: 19364476

Figure Legends

Figure 1. Primary screening and hit validation. A) Representative PASS outputs of active and inactive PS127 molecules on relevant biological activities. **B**) The *in silico* screening pipeline to

uncover additional active novel small molecules. **C**) The top two clusters from MDS analysis. **D**) Scatter plot of cluster 20 (PS127-family), showing all PS127 molecules (blue) and tested compounds (yellow). Three molecules with the strongest cytotoxic activity were labelled. **E**) Cytotoxicity of representative molecules from cluster 20 and cluster 103 at 10 μM on MOLM-13. **F**) Flow chart of a downstream *in silico* screening with the third PASS-predicted activity, autophagy inducer. G) Cytotoxicity comparison of compounds with three PASS-predicted activities. Representative compounds from non-PS127-family were tested at 10 μM in MOLM-13. Bar graphs displayed average of three biological replicates, each of which was represented in data points. Error bars indicated SEM. ANOVA using post-hoc Dunnett's test was used to identify statistical significance. * - $p<0.05$, ** - $p<0.01$, *** - $p<0.001$, ns – not significant.

Figure 2. Synergistic effect of PS127-compounds and commercial chemotherapeutics in MOLM-13. A) Average maximum synergy score of PS127-family compounds and commercial chemotherapeutics: MID, DOX, and ara-C. Red area represented synergy (above 10), grey represented additive (-10 – 10), and green represented antagonistic effects (< -10). **B**) Representative synergy plot of MOLM-13 cells (left) or PBMCs (right) with PS127_4 and MID. **C**) Comparison of MOLM-13 and PBMCs viability upon monotherapy or combined treatments with PS127_4 and MID. Bar graphs (normalized mean ± SEM) represented viability in MOLM-13 cell lines or PBMCs at maximum synergy condition. **D**) Representative synergy plot of MOLM-13 cells (left) or PBMCs (right) with PS127_4 and DOX. **E**) Comparison of MOLM-13 and PBMCs viability upon monotherapy or combined treatments with PS127_4 and DOX. Bar graphs (normalized mean ± SEM) represented viability in MOLM-13 cell lines or PBMCs at maximum synergy condition. Black asterisks indicated comparison of AML cells vs. healthy PBMCs under

the same combinatorial treatment conditions. Pink asterisks indicated significantly lower survival under combinatorial treatment compared to single PS127-family compound treatment; Blue asterisks indicated significantly lower survival under combinatorial treatment compared to a single MID treatment. Significance was assessed via ANOVA using post-hoc Dunnett's test. * - $p<0.05$, ** - $p<0.01$, *** - $p<0.001$, ns – not significant.

Figure 3. Synergistic effect of PS127-compounds with MID in other AML cell lines. A) Average maximum synergy of PS127-family compounds and MID in other AML cell lines, MV4;11 and OCI-AML2. Red area indicated synergy (greater than 10), grey indicated additive (-10 – 10), and green indicated antagonistic effects (less than - 10). **B**) Representative synergy landscape of MV4;11 cells (left) or healthy PBMCs (right) with PS127_4 and MID. **C**) Comparison of MV4;11 and PBMCs viability upon monotherapy or combined treatments with PS127_4 and MID. Bar graphs (normalized mean ± SEM) represented viability in MV4;11 cell lines or PBMCs at maximum synergy condition. Black asterisks indicated comparison of AML cells vs. healthy PBMCs under the same combinatorial treatment conditions. Pink asterisks indicated significantly lower survival under combinatorial treatment compared to single PS127-family compound treatment; Blue asterisks indicated significantly lower survival under combinatorial treatment compared to a single MID treatment. Significance was assessed via ANOVA using post-hoc Dunnett's test. * - $p<0.05$, ** - $p<0.01$, *** - $p<0.001$, ns – not significant.

Figure 4. Validating predicted activities of PS127-treatment in MOLM-13. A) A representative flow cytometry analysis of apoptotic cells induced by PS127E (8 μM, blue) or DMSO (red) for 24 hours. Apoptotic assay was determined using flow cytometry with Annexin

V-FITC/PI/Hoechst staining. **B**) Flow cytometry quantification of cell populations upon PS127-molecule treatment compared to DMSO following annexin V-FITC/PI staining. Apoptotic cells were detected by annexin V-FITC$^+$/PI$^-$ and annexin V-FITC$^+$/PI$^+$, while non-apoptotic dead cells were indicated by annexin V-FITC$^-$/PI$^+$ and live cells were annexin V-FITC$^-$/PI$^-$. Bar graphs indicated the average percentage of cell population and error bars displayed standard error mean. Significance levels represented comparison of PS127-induced apoptotic cells to DMSO. Grey, green and yellow asterisks displayed statistical significance to control of the same group: live, late apoptotic, and non-apoptotic dead cells, respectively. **C**) Antagonistic interactions between 3-MA and PS127 family. A representative landscape of PS127E and 3-MA treatment (left) and the average antagonistic scores of other PS127-molecules were summarized in table (right). **D**) The effect of PS127-molecules on TrxR activity. **E**) Changes of GSH to GSSG ratio indicated the impact of PS127-molecules on GSR activity. All results were representative of at least three biological replicates, each of which was shown as data point in boxplot. Statistical significance was assessed via ANOVA using post-hoc Dunnett's test. * - $p<0.05$, ** - $p<0.01$, *** - $p<0.001$, ns – not significant.

Figure 5. The effect of PS127-induced cytotoxicity on redox metabolism and ROS level in MOLM-13. A) The PS127E-induced cytotoxicity for 72 hours was rescued by various ROS scavengers. **B**) Changes of cellular and mitochondrial ROS upon PS127E treatment in the presence of ROS scavengers was assessed using flow cytometry. Representative histograms of DHE$^+$ (left panel) and MitoSOX Red$^+$ (right panel) population in the presence of ROS scavengers compared to negative control. Peak with dashed lines indicate control treatment or in absence of PS127-

molecule, while solid lines represent treatment with PS127-molecule. **C**) Quantification of ROS in the presence of ROS scavengers. ROS level was indicated by median fluorescence intensity (MFI) of ROS staining dye. **D**) DSF with GSR was performed to determine changes in melting temperature (Tm). PS127_4, PS127_9, PS127_10, and PS127E were found to significantly change the Tm of GSR, indicating compound-enzyme binding. 125_1 = active non-PS127-family compound, 127H = previously identified inactive PS127 analog, 2-AAPA = GSR inhibitor control. All statistical significance was assessed via ANOVA using post-hoc Dunnett's test, comparing each treatment against the no ROS scavenger group. * - $p<0.05$, ** - $p<0.01$, *** - $p<0.001$, ns – not significant.

Figure 6. Evaluation of PASS-predicted activities in 125_1 and their mechanistic activity to induce cell death. A) Quantification of apoptotic cells upon 125_1 treatment in MOLM-13, indicated by Annexin V/PI staining. **B**) Antagonistic interactions between 3-MA and 125_1. **C**) Cytotoxicity upon 125_1 treatment was rescued by GSH, but not other ROS scavengers. **D**) Treatment of 125_1 changed the total and mitochondrial ROS level. Representative histograms of DHE^+ (left panel) and $MitoSOX^+$ (right panel) population upon 125_1 treatment in the presence of ROS scavengers compared to negative control. Peak with dashed lines indicated control treatment or in absence of PS127-molecule, while solid lines represented treatment with PS127-molecule. **E**) Quantification of total (upper panel) and mitochondrial (below panel) ROS level in the presence of ROS scavengers. ROS level was indicated by MFI of ROS staining dye. **F**) DSF with GSR was performed to determine changes in melting temperature (Tm). 125_1 significantly increased the Tm of GSR, indicating compound-enzyme binding. **G**) Compound 125_1 had synergistic effect with MID in MOLM-13. Synergy score was calculated using the Bliss model.

Statistical significance of apoptotic cells and ROS level was assessed via ANOVA using post-hoc Dunnett's test, comparing each treatment against the no ROS scavenger group. Significance level of DSF was determined using Student's T-test. * - $p<0.05$, ** - $p<0.01$, *** - $p<0.001$, ns – not significant.

Figure 7. Compounds with all three PASS-predicted activities interfered with mitochondrial biogenetics. A) The routine oxygen consumption rate (OCR) was measured for treated and non-treated MOLM-13 cells. Cells that were treated with compounds for 3 hours had significantly less oxygen consumption compared to the solvent-control. OCR was normalized to the number of cells per chamber volume. **B**) The steady state ATP level in MOLM-13 was measured after 3 hours of treatment exposure. Total ATP was quantified by dividing the luminescence measurement by the number of live cells. All MOLM-13 cells had a cell viability ≥ 90% before cell lysis occurred to measure total ATP. All statistical significance was assessed via ANOVA using post-hoc Dunnett's test. * - $p<0.05$, ** - $p<0.01$, *** - $p<0.001$, ns – not significant.

Table 1. CC_{50} (mean ± SEM, μM) value of PS127-family compounds in MOLM-13, PBMCs, and H9C2

Compounds	MOLM-13	PBMC	PBMC/MOLM-13 ratio	H9C2	H9C2/MOLM-13 ratio
127_1	>8	>16	ND	ND	ND
127_2	1.62 ± 0.08	4.38 ± 0.30	2.71	>16	ND
127_3	2.41 ± 0.12	9.47 ± 1.56	3.94	>16	ND
127_4	0.33 ± 0.02	5.93 ± 0.53	18.04	5.84 ± 1.59	17.70
127_5	1.15 ± 0.05	7.46 ± 0.33	6.48	>16	ND
127_6	1.05 ± 0.05	8.37 ± 0.70	7.97	>16	ND
127_8	6.03 ± 0.22	>16	> 5.28	>16	ND
127_9	0.59 ± 0.02	9.79 ± 1.41	16.65	9.19 ± 0.88	15.58
127_10	0.39 ± 0.02	7.37 ± 0.61	18.78	3.73 ± 0.10	9.56
127_13	2.15 ± 0.41	>16	> 7.44	>16	ND
127_14	3.68 ± 0.17	>16	> 4.35	>16	ND
127_20	1.41 ± 0.11	2.94 ± 0.43	2.09	>16	ND
127_21	>8	>16	ND	ND	ND
PS127E	0.56 ± 0.09	10.72 ± 1.11	19.14	16.88 ± 2.48	30.14

ND: Not determined

Table 2. CC_{50} (mean ± SEM, μM) of prioritized PS127-family compound in other AML cell lines

Compounds	MOLM-14	MV4;11	THP-2	OCI-AML2
127_4	0.71 ± 0.04	0.73 ± 0.07	0.90 ± 0.07	0.96 ± 0.14
127_9	0.94 ± 0.09	1.38 ± 0.12	1.36 ± 0.06	1.38 ± 0.11
127_10	0.92 ± 0.05	0.80 ± 0.07	0.93 ± 0.04	1.11 ± 0.11
PS127E	1.28 ± 0.09	1.26 ± 0.14	1.23 ± 0.14	2.35 ± 0.23

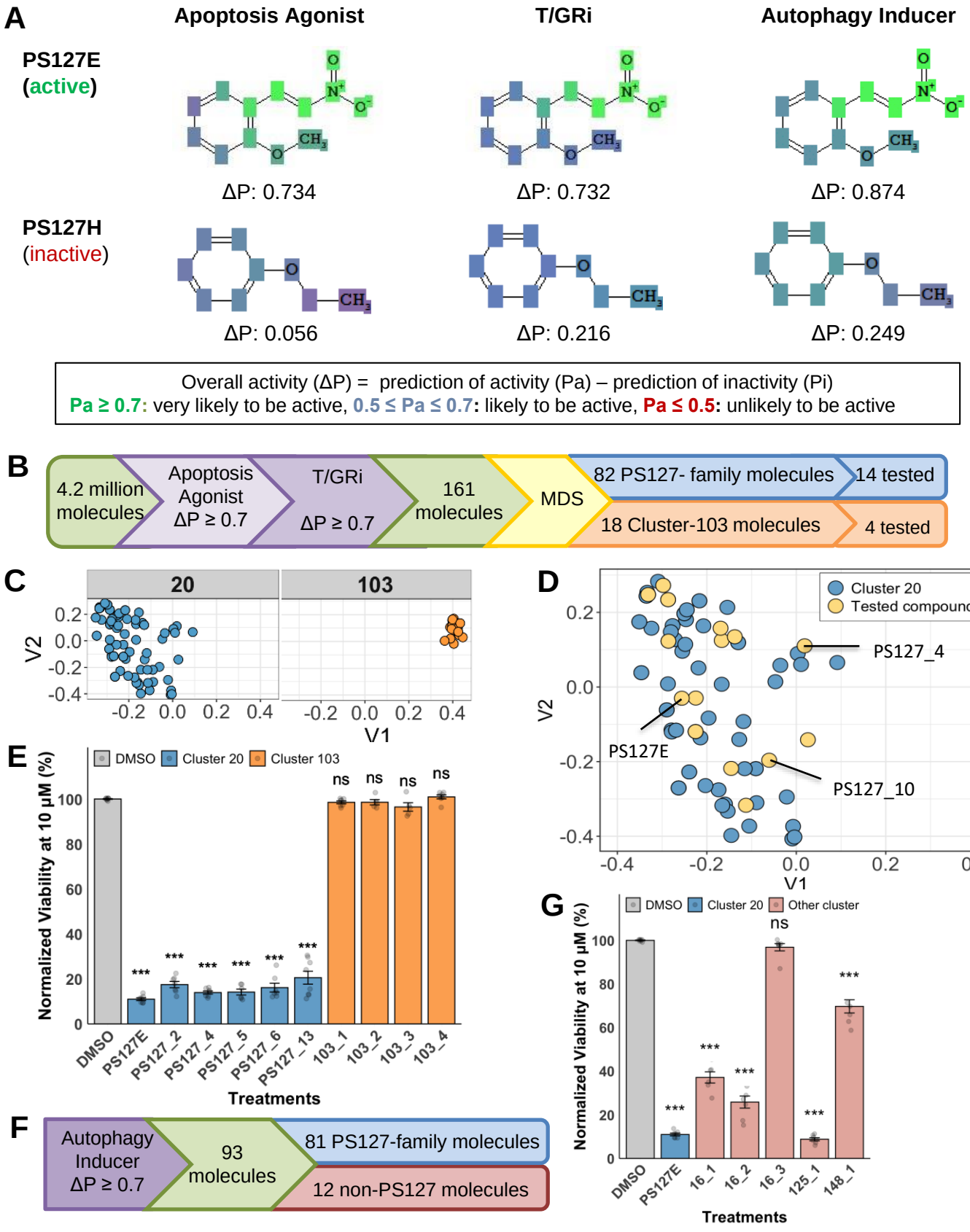
A
Apoptosis Agonist
T/GRi
Autophagy Inducer
PS127E (active)
ΔP: 0.734
ΔP: 0.732
ΔP: 0.874
PS127H (inactive)
ΔP: 0.056
ΔP: 0.216
ΔP: 0.249
Overall activity (ΔP) = prediction of activity (Pa) – prediction of inactivity (Pi)
Pa ≥ 0.7: very likely to be active, 0.5 ≤ Pa ≤ 0.7: likely to be active, Pa ≤ 0.5: unlikely to be active
B
4.2 million molecules
Apoptosis Agonist ΔP ≥ 0.7
T/GRi ΔP ≥ 0.7
161 molecules
MDS
82 PS127- family molecules
14 tested
18 Cluster-103 molecules
4 tested
C
20
103
V2
V1
D
Cluster 20
Tested compounds
PS127_4
PS127E
PS127_10
V2
V1
E
DMSO
Cluster 20
Cluster 103
Normalized Viability at 10 µM (%)
ns
***
DMSO
PS127E
PS127_2
PS127_4
PS127_5
PS127_6
PS127_13
103_1
103_2
103_3
103_4
Treatments
F
Autophagy Inducer ΔP ≥ 0.7
93 molecules
81 PS127-family molecules
12 non-PS127 molecules
G
DMSO
Cluster 20
Other cluster
Normalized Viability at 10 µM (%)
DMSO
PS127E
16_1
16_2
16_3
125_1
148_1
Treatments

Figure 1

A

PS127 compounds	MID	DOX	ara-C	Synergistic	Not Synergistic
127_4	41.02 ± 6.79	26.04 ± 2.52	17.13 ± 1.49	High (>30)	Additive (-10 – 10)
127_10	34.4 ± 3.07	14.75 ± 1.02	16.38 ± 1.88	Medium (20 - 30)	Antagonistic (< -10)
PS127E	39.10 ± 4.42	18.97 ± 2.50	11.10 ± 0.66	Low (>10 - 20)	

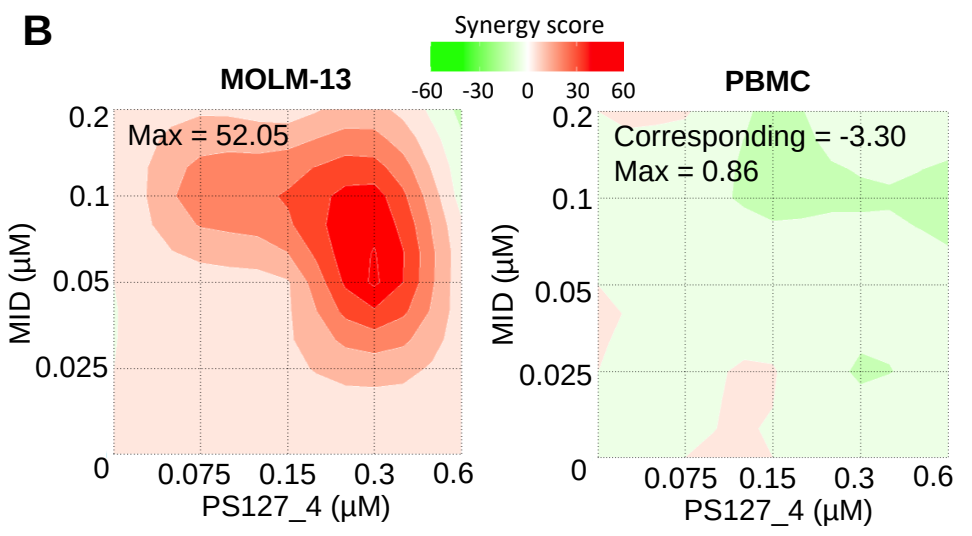

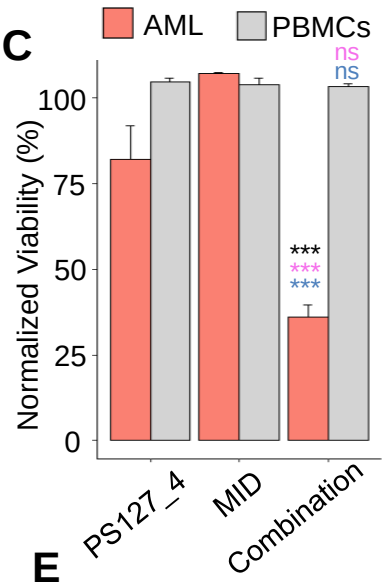

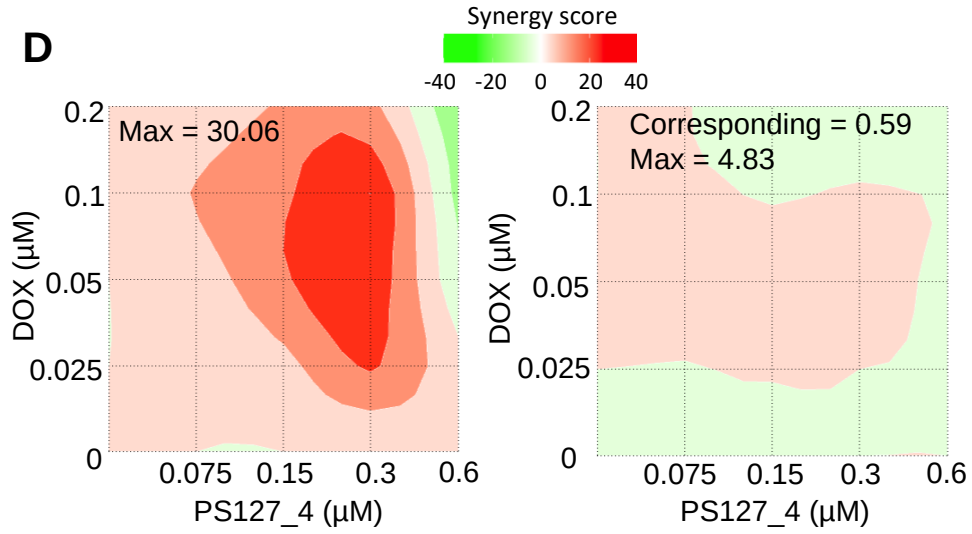

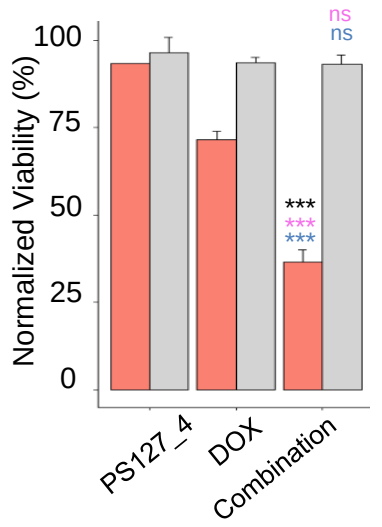

Figure 2

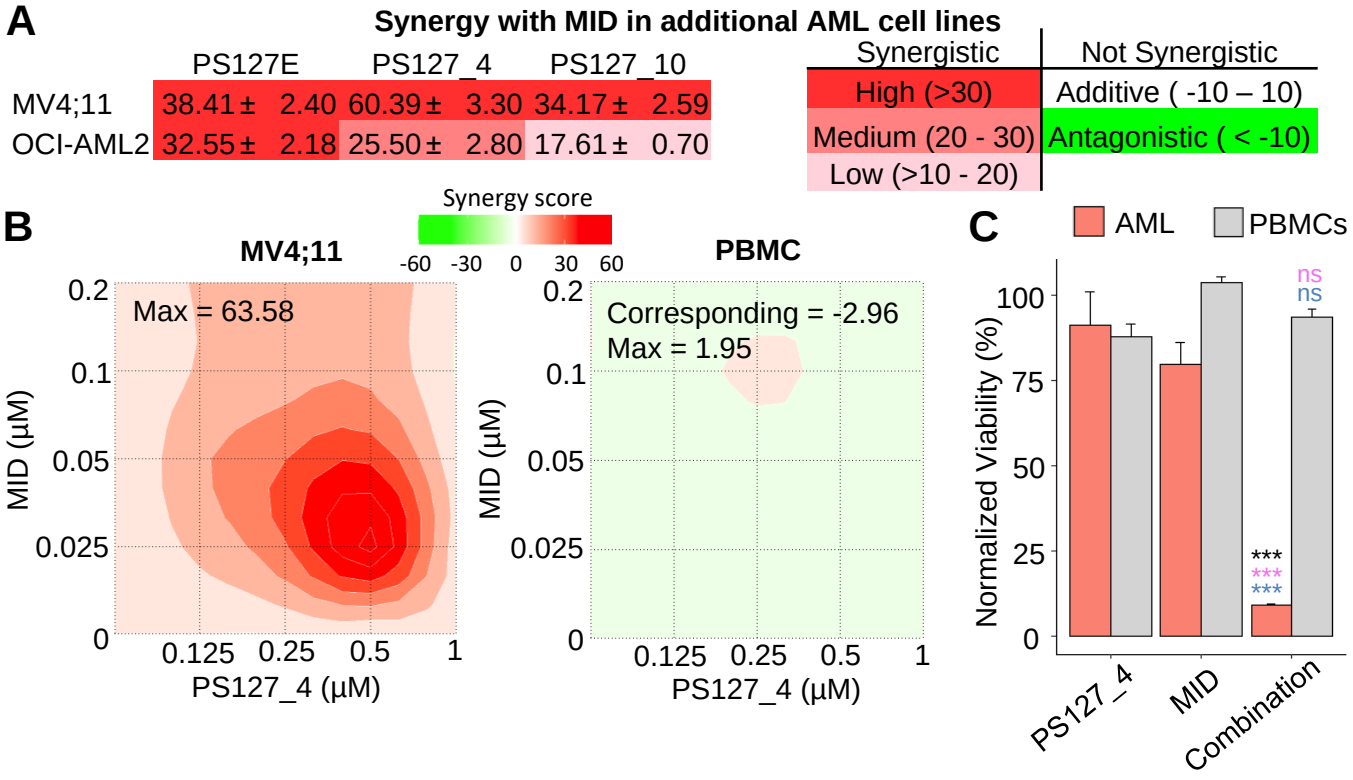
A
Synergy with MID in additional AML cell lines
PS127E
PS127_4
PS127_10
MV4;11
38.41 ± 2.40
60.39 ± 3.30
34.17 ± 2.59
OCI-AML2
32.55 ± 2.18
25.50 ± 2.80
17.61 ± 0.70
Synergistic
Not Synergistic
High (>30)
Additive (-10 – 10)
Medium (20 - 30)
Antagonistic (< -10)
Low (>10 - 20)
B
Synergy score
-60 -30 0 30 60
MV4;11
Max = 63.58
PBMC
Corresponding = -2.96
Max = 1.95
MID (µM)
PS127_4 (µM)
0.2
0.1
0.05
0.025
0
0.125 0.25 0.5 1
C
AML
PBMCs
Normalized Viability (%)
100
75
50
25
0
ns
ns
***
***
***
PS127_4
MID
Combination

Figure 3

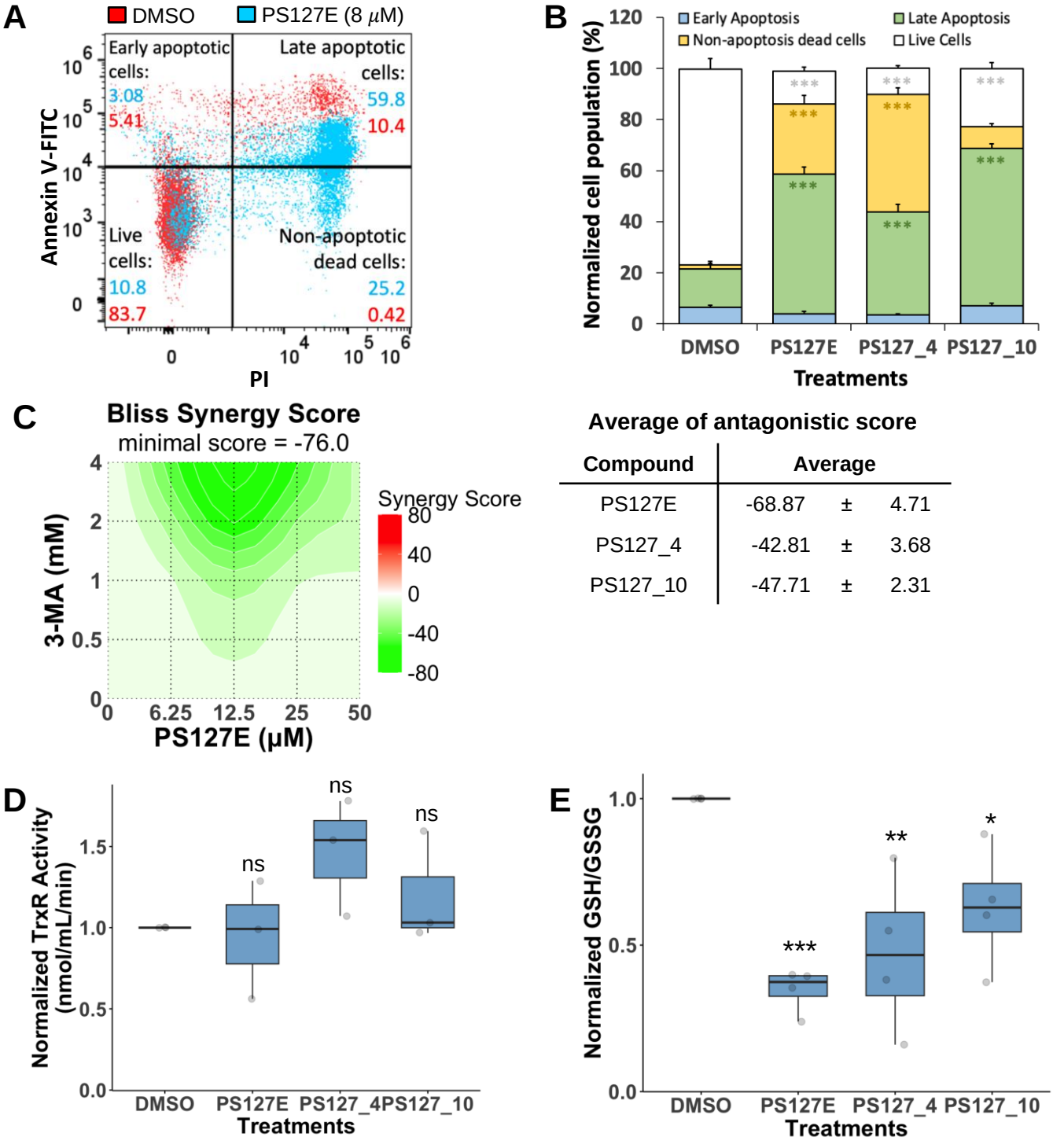
A
DMSO
PS127E (8 μM)
Early apoptotic cells:
3.08
5.41
Late apoptotic cells:
59.8
10.4
Live cells:
10.8
83.7
Non-apoptotic dead cells:
25.2
0.42
Annexin V-FITC
PI
B
Early Apoptosis
Late Apoptosis
Non-apoptosis dead cells
Live Cells
Normalized cell population (%)
DMSO
PS127E
PS127_4
PS127_10
Treatments
C
Bliss Synergy Score
minimal score = -76.0
Synergy Score
3-MA (mM)
PS127E (μM)
Average of antagonistic score
Compound
Average
PS127E
-68.87 ± 4.71
PS127_4
-42.81 ± 3.68
PS127_10
-47.71 ± 2.31
D
Normalized TrxR Activity (nmol/mL/min)
ns
DMSO
PS127E
PS127_4
PS127_10
Treatments
E
Normalized GSH/GSSG
DMSO
PS127E
PS127_4
PS127_10
Treatments

Figure 4

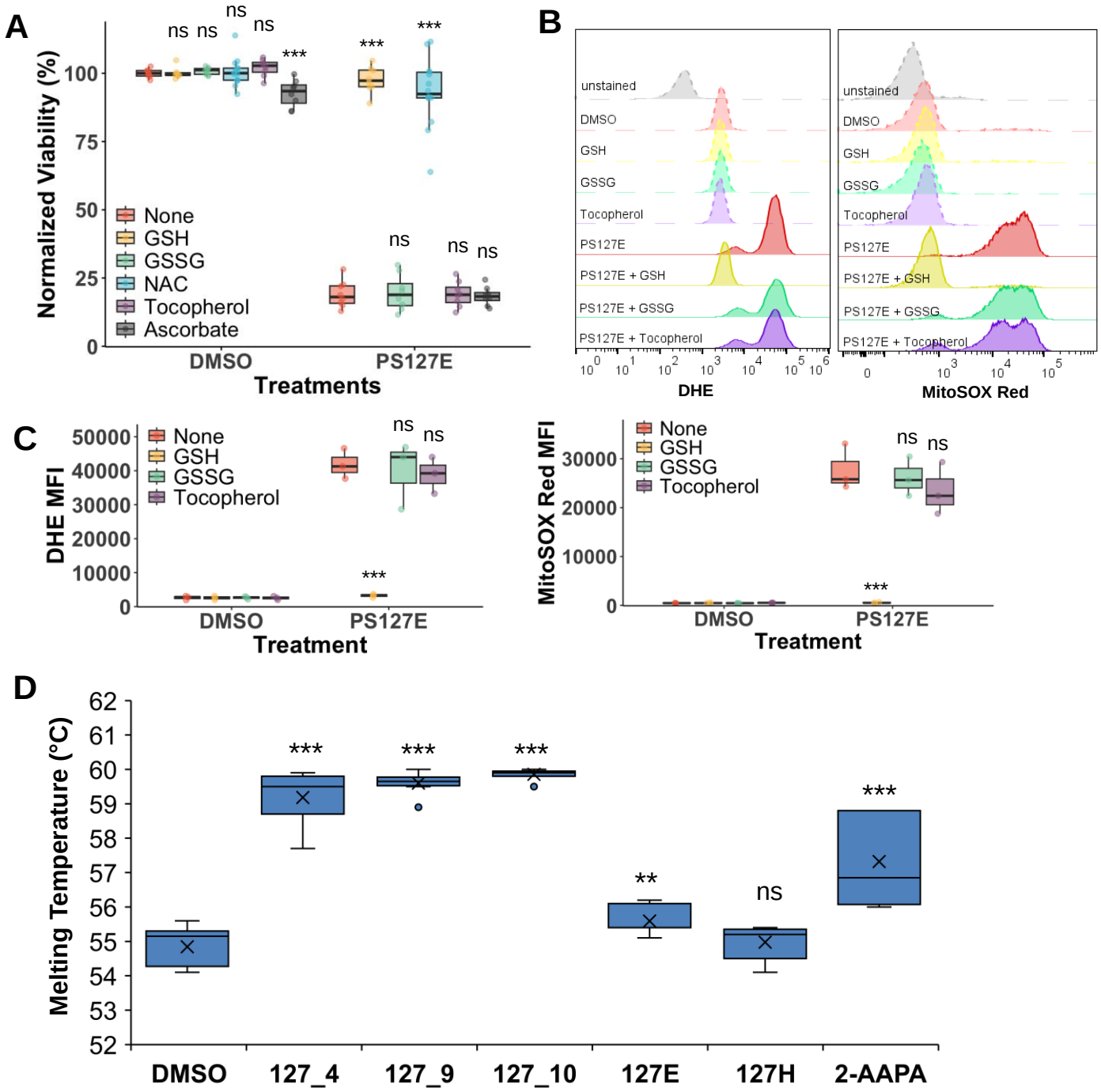
A
Normalized Viability (%)
None
GSH
GSSG
NAC
Tocopherol
Ascorbate
DMSO
PS127E
Treatments
B
unstained
DMSO
GSH
GSSG
Tocopherol
PS127E
PS127E + GSH
PS127E + GSSG
PS127E + Tocopherol
DHE
MitoSOX Red
C
DHE MFI
Treatment
MitoSOX Red MFI
D
Melting Temperature (°C)
DMSO
127_4
127_9
127_10
127E
127H
2-AAPA

Figure 5

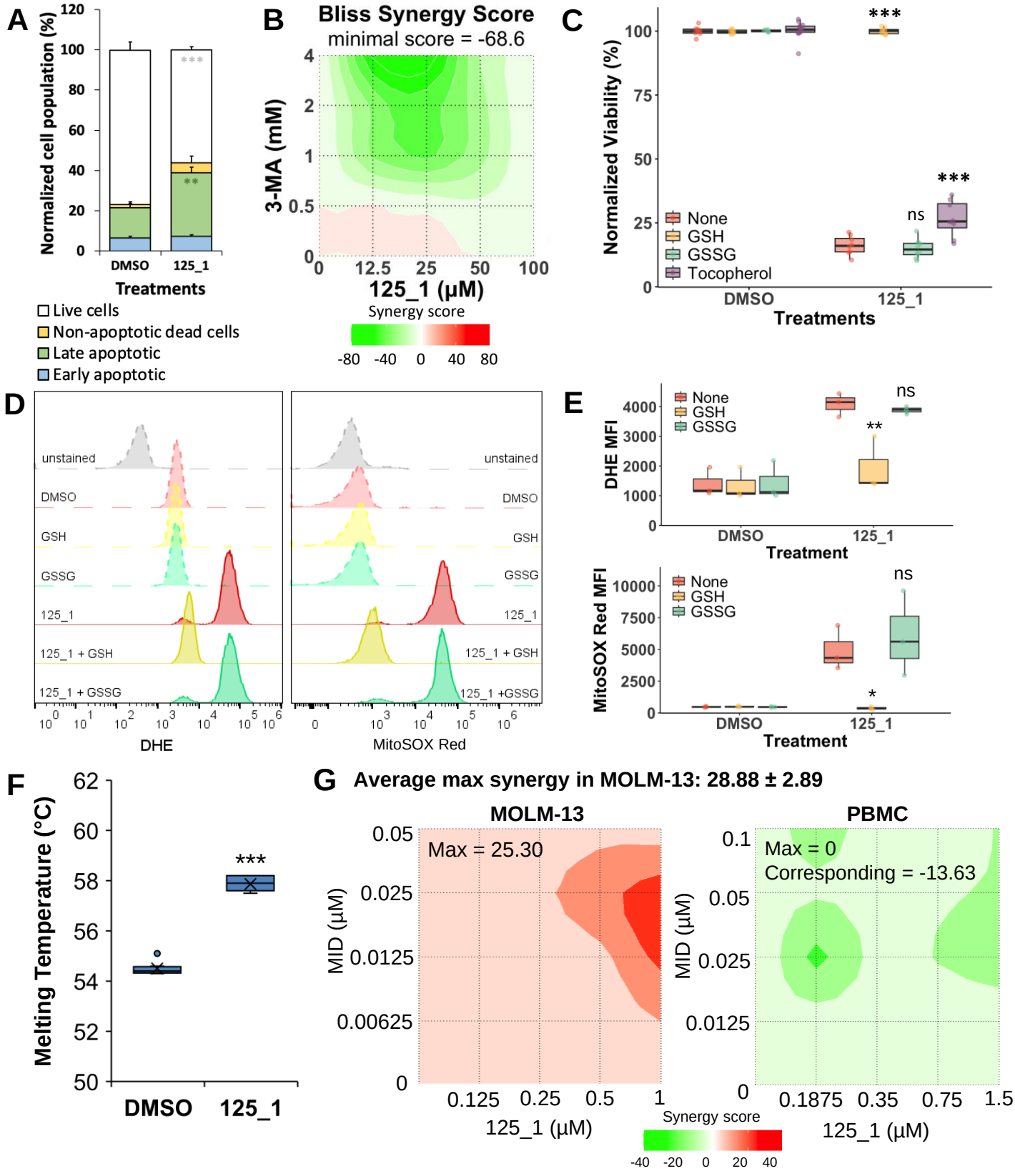
A
Normalized cell population (%)
Treatments
DMSO
125_1
Live cells
Non-apoptotic dead cells
Late apoptotic
Early apoptotic
B
Bliss Synergy Score
minimal score = -68.6
3-MA (mM)
125_1 (μM)
Synergy score
C
Normalized Viability (%)
None
GSH
GSSG
Tocopherol
ns
D
unstained
DMSO
GSH
GSSG
125_1
125_1 + GSH
125_1 + GSSG
DHE
MitoSOX Red
E
DHE MFI
MitoSOX Red MFI
Treatment
F
Melting Temperature (°C)
G
Average max synergy in MOLM-13: 28.88 ± 2.89
MOLM-13
PBMC
Max = 25.30
Max = 0
Corresponding = -13.63
MID (μM)
125_1 (μM)
Synergy score

Figure 6

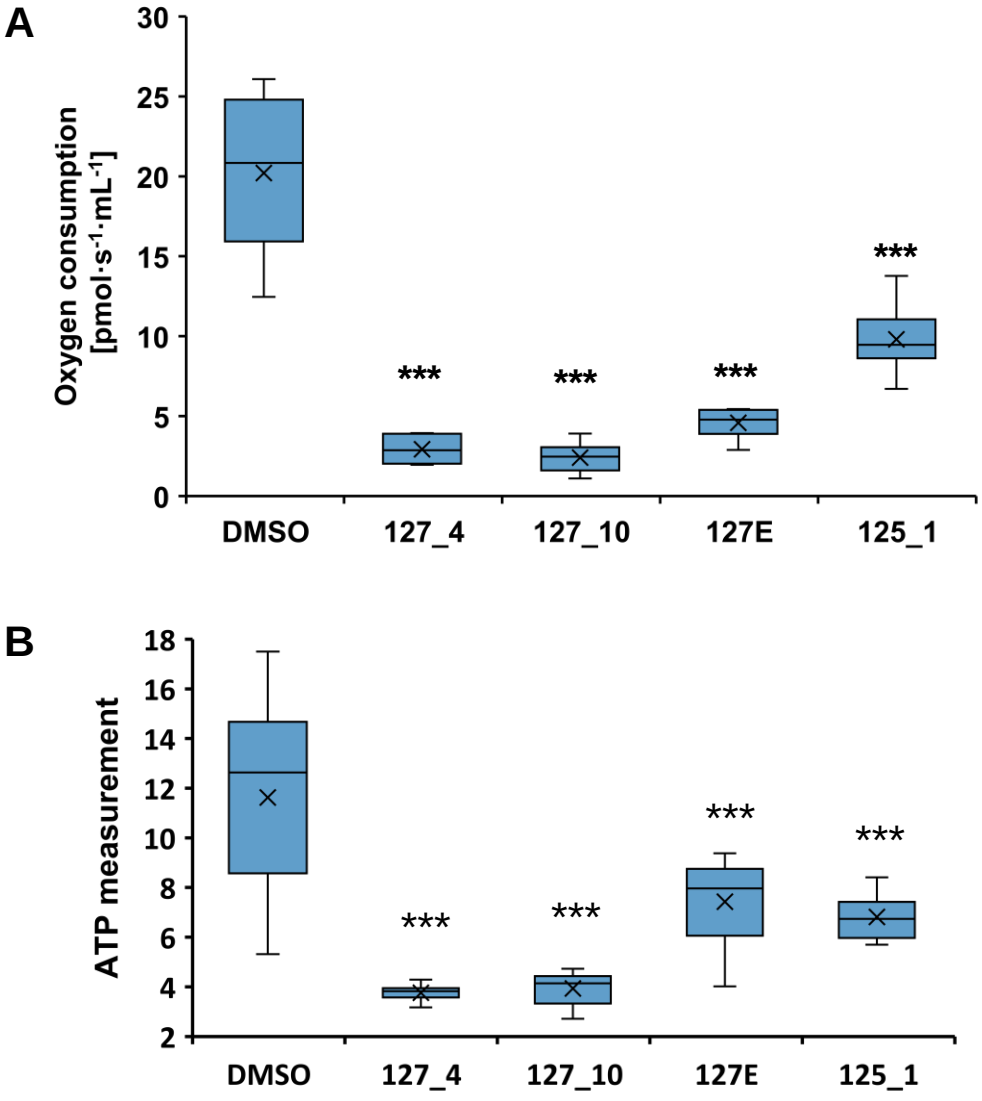
A
Oxygen consumption [pmol·s-1·mL-1]
30
25
20
15
10
5
0
***
***
***
***
DMSO
127_4
127_10
127E
125_1
B
ATP measurement
18
16
14
12
10
8
6
4
2
***
***
***
***
DMSO
127_4
127_10
127E
125_1

Figure 7